# Near-Fault Earthquake Ground Motion and Seismic Isolation Design

Mustafa Erdik[1]([✉]), Bahadır Şadan[2], Cüneyt Tüzün[3], Mine B. Demircioglu-Tumsa[4], Ömer Ülker[4], and Ebru Harmandar[5]

[1] Department of Earthquake Engineering, Boğaziçi University, Istanbul, Turkey
erdik@boun.edu.tr
[2] Department of Civil Engineering, MEF University, Istanbul, Turkey
[3] Department of Civil Engineering, Yaşar University, Izmir, Turkey
[4] Turkish Earthquake Foundation, Istanbul, Turkey
[5] Department of Civil Engineering, Sıtkı Kocman University, Muğla, Turkey

**Abstract.** Seismic isolation is one of the most reliable passive structural control techniques with adequately established standards for the earthquake protection of structures from earthquakes. However, it has been shown that the seismic isolation systems may not function the best for the near-fault ground motions, since in the proximity of a capable fault, the ground motions are significantly affected by the rupture mechanism and may generate high demands on the isolation system and the structure. In fact, several earthquake resistant design codes state that the seismically isolated structures located at near-fault sites should be designed by considering larger seismic demands than the demand on structures at far-field sites. When the fault ruptures in forward direction to the site most of the seismic energy arrives in coherent long-period ground velocity pulses. The ground-motion prediction equations (GMPEs) typically cannot account for such effects with limited distance metrics and lack adequate data at large magnitudes and near distances. For the reliable earthquake design of the isolated structure in near fault conditions that meets the performance objectives, the 3D design basis ground motion(s) need to be appropriately assessed. Measures in the design of the isolation system, such as modifications in the stiffness and damping characteristics, as well as in the limitation of vertical effects are needed. The behavior of the base-isolated buildings under near-fault (NF) ground motions with fling-step and forward-directivity characteristics are investigated with a rational assessment of design-basis near-fault ground motion, are investigated in a parametric format. The parametric study includes several variables, including the structural system flexibility; number of stories; isolation system characteristic (yield) strength, and the isolation periods related to the post-elastic stiffness. Furthermore, the effect of additional damping by viscous dampers were tested for some selected cases. Important findings observed from the parametric performance results and the overall conclusions of the study are provided.

**Keywords:** Base-isolated buildings · Fling-step · Forward-directivity · Near-fault ground motions · Pulse period

# 1 Introduction

It is essential to maintain the functionality of critical structures to form resilient societies after moderate-to-severe ground shaking. Seismic isolation of structures is a mature technique for the design of new and retrofit of existing structures. The earthquake-resistant design of seismically isolated structures can entail sophisticated analysis for the accurate estimation of seismic demands in near-fault regions, and the most accurate estimate of seismic demands of isolated structures can be obtained through nonlinear response history analysis.

Near-fault ground motions have distinguishing characteristics that are related to the faulting mechanism, location of the hypocenter, and direction of rupture propagation relative to the location of the site.

This study investigates the influence of near-fault ground motions on seismically isolated structures by considering their well-known characteristics and provides state-of-the-practice design methodologies for such cases. The near-fault ground motion characterization is reviewed for the proper seismic isolation applications for building-type structures. A set prototype building is exposed to multi-component earthquake ground motions with pulse content in near-fault regions to address problems associated with close proximity to the active faults. Isolation units with a large displacement capacity and sufficient restoring force capacity need to be elaborately selected to accommodate the large displacement demands of these structures.

Earthquakes can be described as a shear dislocation phenomenon that starts to radiate from the focus of the source to the site. Damaging effects of the earthquake emerge when the frequency content of the seismic input motion coincides or is in close range with the fundamental frequency of vibration. Seismic isolation application conceptually aims to decouple structures from the horizontal components of earthquake ground motion by shifting the fundamental period of vibration beyond the damaging range of frequencies. Period shift and the consequential accommodation of displacement demands are generally provided by the installation of elastomeric or curved surface slider bearings to structures. In addition, seismic isolators are used to reduce the acceleration and/or drift response of buildings in order to improve their post-earthquake functionality. Effects of a seismic isolation system on damping and the fundamental period of vibration are shown in Fig. 1.

Prediction of displacement demands in seismically isolated structures is crucial since it has been identified as an important performance indicator. Displacement spectra constitute the main component of displacement-based design (DBD) procedures as per the recommendations developed by Priestly et al. [58]. In some codes, the establishment of displacement spectra is based on the assumption of steady-state behavior. Some standards (e.g., CEN, [20]) provide the characteristic shape of the displacement spectrum on this basis. Apart from the code-based displacement spectra, ground motion prediction equations can be utilized for the computation of displacement spectra. Among others, Bommer and Elnashai [11], Faccioli et al. [31], and Cauzzi et al. [19] have developed empirical relationships for the prediction of spectral displacement amplitudes based on available strong motion data that also contain near-fault data.
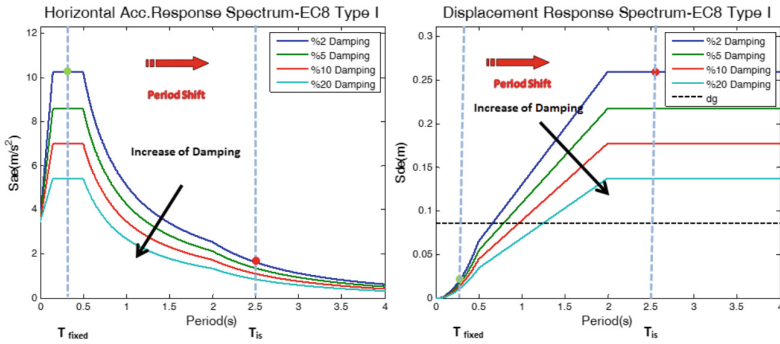
**Fig. 1.** Effects of seismic isolation on acceleration and displacement spectra.

## 2 Near-Fault Ground Motions

### 2.1 Background

Distinctive characteristics of near-fault ground motions have been realized through the dense ground motion arrays deployed in the vicinity of active faults. Near-fault seismic ground motions are frequently characterized by intense velocity and displacement pulses of relatively long duration, which clearly distinguishes them from typical far-field ground motion records.

Near-fault ground motions contain coherent and orientation-dependent effects at intermediate and long periods, such as rupture directivity pulses and fling steps. Extensive damage to some structures in near-fault regions is attributed to these particular features. Earthquakes in close proximity to faults, such as the 1992 Erzincan-Turkey, 1992 Landers-California, 1994 Northridge-California, 1996 Kobe-Japan, 1999 Kocaeli-Turkey, 1999 Chi Chi-Taiwan, and 2011 Christchurch-New Zealand earthquakes, have provided valuable information about the characteristics of this type of ground motions.

### 2.2 Characteristics of Near-Fault Ground Motions

The large amount of data gathered from site surveys and strong ground motion recordings allowed the earthquake engineering community to understand the near-field effects. It has been recognized that near-source ground motions are dominated by source characteristics and may vary considerably depending on the characteristics of rupture propagation. Post-earthquake observations from major earthquakes indicate that extensive damage to structures is attributed to particular characteristics of near-source records within 0–15 km distance to fault rupture. The main distinctive characteristics of near-source earthquakes can be listed as directivity and fling effects which are associated with long period pulse content and large vertical ground motions.

#### 2.2.1 Directivity Effects

Directivity effects have been studied by numerous researchers as a cause of velocity pulses (e.g., Hall et al. [40]; Somerville and Graves [68]). Rate and duration are the two

important factors that influence the large ground displacement demands. The duration of these displacements is closely related to the characteristic slip time on the fault (Heaton [41]).

In near-fault conditions, two distinct displacement patterns may be observed as a consequence of the rupture process (Sommerville et al. [71]). The first displacement pattern associated with double-sided velocity pulses is generally observed in the fault normal component of strike-slip motions. The so-called Fault-Normal Forward Directivity Effect occurs when the fault rupture propagates toward a site with a rupture velocity that is approximately equal to the shear wave velocity. In this case, most of the energy arrives coherently in a single, intense, relatively long-period pulse at the beginning of the record. Near-field locations with dip-slip faulting mechanisms can additionally experience hanging wall effects as well.

The second displacement pattern is linked with the so-called Fault-Parallel Fling Step action that accounts for permanent displacement offsets. Fling Effect (permanent translation) appears in the form of step displacement and one-sided velocity pulse in the strike-parallel direction for strike-slip faults or in the strike-normal direction for dip-slip faults.

Figure 2 (after Mavroedis and Papageorgiu [48]) illustrates the fault normal (forward directivity, ARC Station record) and fault parallel (fling step, SKR Station record) ground motion associated with the 1999 Izmit (Kocaeli) earthquake (Mw7.4) in Turkey. A simple pulse-type ground motion model (black trace) was fitted to the recorded ground motions (gray trace). Time histories of displacement, velocity, and acceleration are illustrated.
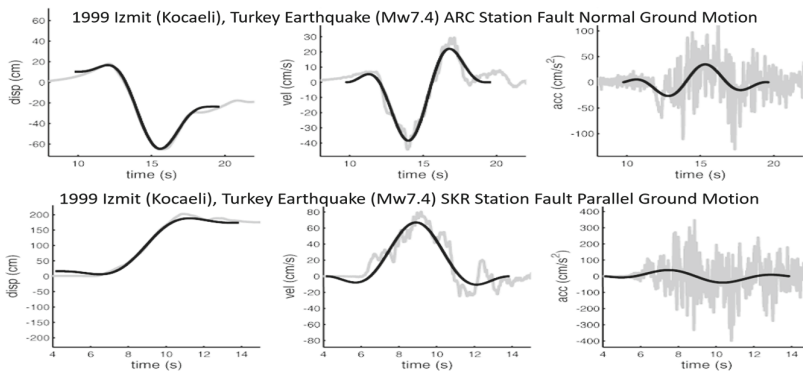


**Fig. 2.** 1999 Izmit (Mw7.4) earthquake, fault normal and fault parallel ground motion associated with the in Turkey (after Mavroedis and Papageorgiu [48]).

### 2.2.2 Near-Fault Vertical Ground Motion

The peak value of the vertical component of earthquakes may exceed its horizontal counterparts in the vicinity of the active faults.

Xinle et al. [79] have investigated the characteristics of near-fault vertical ground motions. The vertical to horizontal spectral ratios obtained from 130 sets of selected

free-field near-fault ground motion indicates that for a spectral period of less than 0.1 s and greater than about 2 s, the spectral ratios for different pulse period ranges are close to 1. The largest spectral ratio of about 1.3 occurs for pulse periods less than 3 s.

Studies of the vertical/horizontal (V/H) spectral amplitude ratios of ground motion (e.g., Bozorgnia and Campbell [12]; Gülerce et al. [38]) have shown the following important characteristics:

(1) The V/H spectral ratio is sensitive to spectral period, fault distance, local site conditions, and earthquake magnitude and has a distinct peak at short spectral periods (0.05–010 s) that increases with decreasing soil stiffness;

(2) At short spectral periods in near-fault conditions, the (V/H) spectral ratio exceeds unity for soft soil sites since the nonlinearity of site response is stronger in the horizontal component than in the vertical component.

(3) The V/H spectral ratio is generally less than 2/3 at mid-to-long periods since the vertical ground motion attenuates at a higher rate (which increases with decreasing distance from the earthquake source) than horizontal ground motion.

Figure 3 (after Gülerce et al. [38]) illustrates the median V/H ratio for a vertical strike-slip earthquake at a 5 km distance from the fault for (a) rock sites (VS30 = 760 m/s) and (b) soil sites (VS30 = 270 m/s).
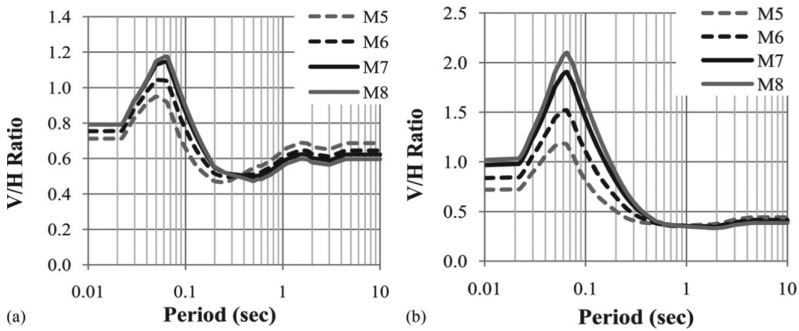


**Fig. 3.** Median V/H ratio for a vertical strike-slip earthquake at a 5 km distance from the fault for (a) rock sites (NEHRP B/C, $V_{S30}$ = 760 m/s) and (b) soil sites (NEHRP D, $V_{S30}$ = 270 m/s) (after Gülerce et al. [38]).

The vertical component of the ground motion is described in EN1998-1 (EC8) by an acceleration response spectrum, Sve, denoted as the "vertical elastic response spectrum." The spectrum is anchored to the value of the peak vertical acceleration $a_{vg}$. For Type-1 earthquakes, the maximum 5% damped spectrum amplitude of the vertical elastic response spectrum is 1.08 times the corresponding horizontal spectral amplitude regardless of earthquake magnitude, distance, and site class.

In ASCE 7-22 [7], Chapter 11.9.2 provides the definition of the $MCE_R$ Vertical Response Spectrum. The vertical spectral amplitude changes as a function of the $C_V$ (Vertical Coefficient) which is tabulated (Table 11.9-1) as a function of the site class

and short period horizontal spectral amplitude ($S_{MS}$). The maximum 5% damped vertical spectral amplitude is 1.58 times the corresponding horizontal spectral amplitude (RotD50), the period ranges of 0.05–01 s for SMS >= 2 and for NEHRP Site Class D.

From Fig. 3, it can be seen that for near-fault conditions, large magnitudes, and soft soil sites, the maximum vertical spectral amplitude can exceed twice the corresponding horizontal spectral amplitude (GeoMean, RotD50) in short periods (0.05–0.1 s). As such, isolated structures in near-fault conditions (especially on the hanging wall side of reverse and oblique faults) are highly vulnerable and require careful consideration of the vertical ground motion excitation for design. Especially, isolation units with relatively low tributary gravity load, and isolation units located below columns that form part of the lateral force-resisting system, can have net uplift or tensile displacements caused by combined large vertical ground motion accelerations and global overturning, thereby inducing high impact forces on the structure and jeopardizing the stability of the isolation units.

## 2.3   Analysis of the Near-Fault Ground Motion

The current state of knowledge for the quantification of forward directivity effects associated with near-fault ground motion can be incorporated into the analysis and design of structures by utilizing different approaches that involve the frequency domain (response spectra) and time domain (ground motion) modifications.

### 2.3.1   Response Spectra Associated with Near-Fault Ground Motion

This response spectrum method is used for the specification of response spectra and the selection of time-histories that are compatible with it. This approach relies on the amplification of the spectral ordinates of the conventional design basis spectrum to incorporate the near-fault effects. In this connection, two different spectra may need to be constructed to account for the fault-normal and fault-parallel ground motion components. Empirical spectral amplification factors are determined on the basis of source and distance relationships of the ruptured fault. They are generally independent of site conditions and ground motion intensity.

In the response spectrum method, generally, an empirical model of rupture directivity effects that utilizes spectral amplification factors, such as those originally proposed by Somerville et al. [71], is considered. Somerville's model uses the length ratio ($X = s/L$) and width ratio ($Y = d/W$), respectively, for strike-slip and dip-slip faulting mechanisms. The azimuth and zenith angles are denoted respectively by $\theta$ and $\varphi$, as illustrated in Fig. 4. In this model, the response spectral ordinates are modified using functions conditional on the directivity of the parameter ($X \cos \theta$ and $Y \cos \phi$) that represent the degree to which the component of fault rupture aligned with the slip direction is towards a site of interest.

The period dependence of the amplitude variations on the average horizontal spectrum, caused by rupture directivity effects shown, are shown in Fig. 5. This figure indicates a transition from coherent to incoherent source radiation and wave propagation conditions at a period of about 0.6 s.
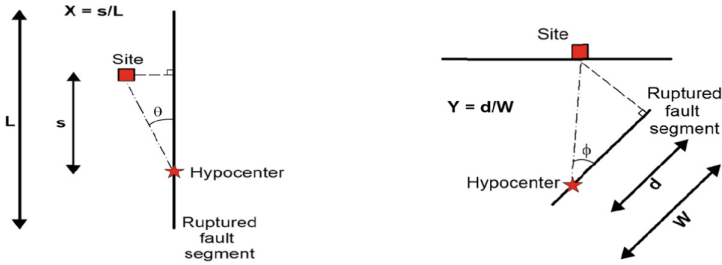
**Fig. 4.** Directivity parameters for strike-slip (plan view) and dip-slip (vertical section) faults defined by Sommerville et al. [71].
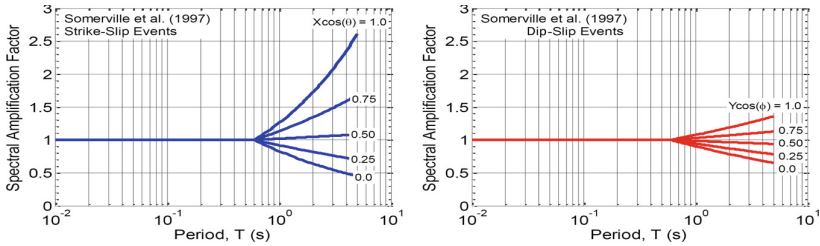


**Fig. 5.** Empirical model of the response spectral amplitude ratio, showing its dependence on period and on the directivity function (X cos θ for strike-slip; Y cos φ for dip-slip faulting) for strike-slip and dip-slip events (Somerville et al. [71]).

Abrahamson [2] has modified the model to saturate the directivity effect for X cos θ > 0.4 and to reduce directivity effects through the use of tapers for distances > 30 km and M < 6.5. Despite the presence of more recent models developed with far larger NGA-West 1 and NGA-West 2 datasets, the experience has been that in practice, the Somerville et al. [71] model in conjunction with the Abrahamson [2] modification continues to be applied to analyze directivity effects on response spectral ordinates (PEER, [57]).

The Final Report of the NGA-West2 Directivity Working Group (PEER, [56]) and the (PEER, [57]) report entitled "Ground-Motion Directivity Modelling for Seismic Hazard Applications" provide a thorough review and applications of the four directivity models developed on the basis of the NGAWest 2 database and on the numerical simulations of large strike-slip and reverse-slip earthquakes. Models by Shahi and Baker, Spudich and Chiou, Rowshandel, Bayless, and Somerville are covered and elaborated in this report. The first three models are explicitly "narrow-band" such that the spectral amplitude change is concentrated around a pulse period, although the Bayless and Somerville model is broadband for a spectral period T > 0.5 s.

The Shahi and Baker [66] Model is specifically aimed at predicting the characteristics of impulsive ground motions often found at short distances from fault ruptures. Since the directivity pulse amplifies spectral acceleration in a narrow band of periods close to the pulse period, their model consists of a wide-band spectral shape plus a superposed narrow-band spectral shape.

The Spudich and Chiou Model uses of Isochrone Directivity Parameter as the predictor. The Chiou and Spudich model introduce the Direct Point Parameter, based on the Isochrone Directivity Parameter, as the directivity predictor, without presenting empirically derived coefficients.

The Rowshandel Model presented in this report is a major modification of Rowshandel [63]. Specifically, rupture length de-normalization is used, and the direction of rupture and slip both contribute to directivity.

Bayless and Somerville's model is an improved version of the classic Somerville et al. [71] model, updated with new data and a better functional form. Major changes include rupture-length denormalization, a modified dependence on site azimuth, use of azimuth tapers to obviate the need for an excluded zone, and extension of the algorithm to allow directivity calculations for complicated, non-contiguous rupture zones. A set of coefficients is presented that is adequate for simulating directivity for several different GMPEs.

For near-fault ground motions, different target spectra should be used for the fault-normal and fault-parallel components to preserve the near-fault features in the process of spectral matching or scaling of ground motions. The Bayless and Somerville model is the only model in this report that predicts directivity for fault-normal and fault parallel motions as well as azimuthally averaged motion. As stated in PEER [57], this model has been implemented in prior work and has a history of project-based peer review. Since this model has a much straightforward application process for professional applications compared to other models, it will be briefly covered.

### Bayless and Somerville Directivity Model

This model is parameterized similarly to the Somerville et al. [71] model (Figs. 4 and 5), except that the dimension of the fault rupturing towards the site is not normalized. The median spectral acceleration from an empirical attenuation relation without directivity effect ($Sa$) can be modified to obtain the spectral acceleration with directivity effects ($Sa_{dir}$) by the following Eq. (1).

$$\ln(Sa_{dir}) = \ln(Sa) + f_D \tag{1}$$

where $f_D$ is the directivity effect given by Eq. (2).

$$f_D = (C_0 + C_1 * f_{geom}) * T_{CD} * T_{Mw} * T_{Az} \tag{2}$$

The directivity effect is quantified as the product of the period and fault-type-dependent constant coefficient, the distance, magnitude, and azimuth tapers, and the geometric directivity predictor ($f_{geom}$), which correlates the directivity effects with the spatial variation of near-fault ground motions. Referring to Fig. 4, $f_{geom}$ is a function of the fraction of the fault rupture surface that lies between the hypocenter and the site (parameter $X$ or $Y$) multiplied by the length or width of the fault (parameter L or W), and the angle between the direction of rupture propagation and the direction of waves traveling from the fault to the site (parameter $\theta$ or $R_x/W$).

### For strike-slip faults:

*Geometric Directivity Predictor:*

$$f_{\text{geom}}(s, \theta) = \log_e(s) * (0.5 \cos(2\theta) + 0.5) \tag{3}$$

*Distance Taper:*

$$
\begin{aligned}
T_{\text{CD}}(R_{\text{rup}}, L) &= 1 & \text{for} & \quad R_{\text{rup}}/L < 0.5 \\
T_{\text{CD}}(R_{\text{rup}}, L) &= 1 - (R_{\text{rup}}/L - 0.5)/0.5 & \text{for} & \quad 0.5 < R_{\text{rup}}/L < 1 \\
T_{\text{CD}}(R_{\text{rup}}, L) &= 0 & \text{for} & \quad R_{\text{rup}}/L > 1.0
\end{aligned} \tag{4}
$$

*Magnitude Taper:*

$$
\begin{aligned}
T_{\text{Mw}}(M_W) &= 1 & \text{for} & \quad M_W > 6.5 \\
T_{\text{Mw}}(M_W) &= 0 & \text{for} & \quad M_W < 5.0 \\
T_{\text{Mw}}(M_W) &= 1 - (6.5 - M!)/1.5 & \text{for} & \quad 5.0 < M_W < 6.5
\end{aligned} \tag{5}
$$

*Azimuth Taper:*

$$T_{\text{Az}}(Az) = 1 \tag{6}$$

The coefficients C0 and C1 of Eq. (2) for different spectral periods are provided in Table 1 for the average horizontal GeoMean (RotD50), fault-normal (FN), and fault-parallel (FP) acceleration spectra. These coefficients represent the smoothed average coefficients derived from fitting residuals from the four 2008 NGA GMPEs. The equations for the predictor and tapers and the coefficients for the dip-slip fault ruptures are provided in PEER [56], similar to those for the strike-slip fault rupture, and will not be included in this paper.

### 2.3.2 Time Domain Representation of Near-Fault Ground Motion

There is growing thinking that the response spectrum method is not fully capable of representing the effects of near-fault pulses. The time domain approach is based on the narrow band representation of the forward directivity and fling-step ground motion through its velocity time history. Strong motion recordings can be assumed to justify that a near-fault pulse is a narrow band pulse, and the near-fault ground motions containing forward rupture directivity and fling step effects may be simple enough to be represented by time domain narrow band pulses through velocity time series with its peak ground velocity, predominant pulse period and expected number of cycles. Needless to say, the expected number of significant pulses depends on the physics of the fault rupture (number of asperities) and cannot be estimated a priori via empirical relationships.

The first work on the pulse-like ground motion was employed by Veletsos and Newmark [77] in connection with the analysis of the response of elastoplastic single-degree-of freedom systems subjected to nuclear explosion generated excitation. The normalized response spectra (Pseudo-Velocity/Maximum Ground Velocity) for different damping ratios that would result from a half–cycle displacement pulse (against $2t_1 f$, where $t_1$ is the ¼ of the displacement pulse duration) and a half–cycle velocity pulse (against $t_d f$, where $t_d$ is the velocity pulse duration) are shown in Fig. 6. Regarding the maximum isolation

**Table 1.** Coefficients of the Bayless and Somerville model for strike-slip ruptures.

| Period (s) | Strike-Slip | | | | | |
| --- | --- | --- | --- | --- | --- | --- |
| | RotD50 | | FN | | FP | |
| | $C_0$ | $C_1$ | $C_0$ | $C_1$ | $C_0$ | $C_1$ |
| 0.5 | 0.000 | 0.000 | 0.000 | 0.000 | 0.000 | 0.000 |
| 0.75 | 0.000 | 0.000 | −0.080 | 0.055 | 0.000 | 0.000 |
| 1 | −0.120 | 0.075 | −0.225 | 0.110 | 0.015 | 0.000 |
| 1.5 | −0.175 | 0.090 | −0.300 | 0.135 | 0.030 | −0.025 |
| 2 | −0.210 | 0.095 | −0.325 | 0.160 | 0.050 | −0.040 |
| 3 | −0.235 | 0.099 | −0.365 | 0.185 | 0.070 | −0.045 |
| 4 | −0.255 | 0.103 | −0.390 | 0.205 | 0.080 | −0.050 |
| 5 | −0.275 | 0.108 | −0.410 | 0.215 | 0.090 | −0.060 |
| 7.5 | −0.290 | 0.112 | −0.420 | 0.220 | 0.100 | −0.070 |
| 10 | −0.300 | 0.115 | −0.425 | 0.225 | 0.108 | −0.071 |
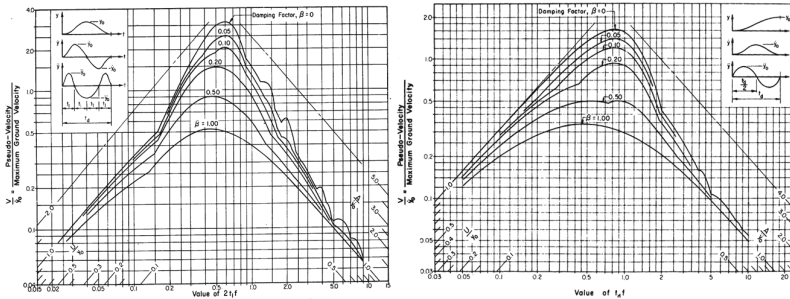


**Fig. 6.** Normalized response spectra for different damping factors that would result from a half–cycle displacement and half–cycle velocity pulses (Veletsos and Newmark [77]).

system displacement, it can be assessed that, for both cases, the spectral displacements vary between 50 and 80% of the peak ground displacement for damping ratios of about 30% for spectral periods between 2 and 5 s.

Assembly of pulse-like ground motions associated with near-fault ground motion was gathered by many researchers to develop quantitative time-domain identification methods for ground motions containing strong velocity pulses.

Sommerville [70, 71] has obtained the magnitude scaling relationships for the fault-normal forward directivity pulse period (T, Eq. (7)) and the peak velocity (PGV, Eq. (8)) in terms of moment magnitude Mw and closest fault distance (R).

$$logT = -3.1 + 0.5Mw \tag{7}$$

$$logPGV = -1.0 + 0.5Mw - 0.5logR \tag{8}$$

Figure 7 provides a simple representation of a simple full cycle forward directivity velocity pulse together with the associated 5% damped response spectra for different pulse periods and velocity pulse amplitudes. For these plots, different combinations of magnitude (Mw) and fault distance (R) combinations as per Eqs. (7) and (8) are considered.
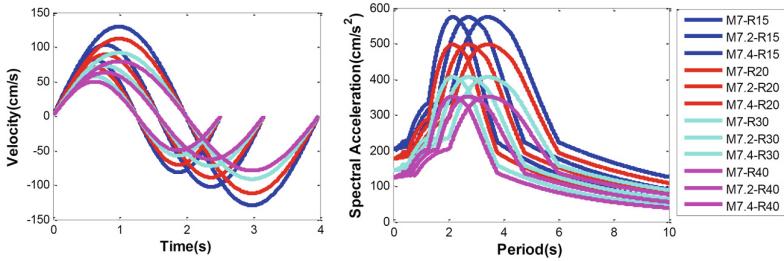


**Fig. 7.** Full-cycle velocity pulse and the corresponding acceleration spectra for forward rupture directivity (near-fault normal ground motion).

In this connection, Baker [8], Tothong et al. [75], and Shahi and Baker [66] have employed a wavelet transform procedure to identify pulse-type signals in a ground motion time history. Bray and Rodriguez-Marek [15], Rodriguez-Marek and Bray [62], and Bray et al. [14] simplify the characterization of near-fault forward directivity motions by using only the peak ground velocity approximate period of the dominant pulse and the number of cycles of pulse motions of the fault-normal component of forward directivity motions. Mavroeidis and Papageorgiou [48] have proposed an analytical model for the representation of near-field strong ground motions, using the Gabor wavelet defined by the four key parameters of the near-source velocity pulses; namely, the amplitude, prevailing frequency, phase, and the oscillatory character of the signal.

For the representation of near-fault records, one can utilize more complicated pulse models such as those derived based on wavelet functions (e.g., Mavroeidis and Papageorgiou [48]; Mavroeidis et al. [49]; Baker [8]); however, for practical design considerations, their calibration is rather difficult due to the presence of supplementary parameters in the definition of wavelet functions. The normalized displacement spectra of fling-step pulse actions are investigated by Faccioli et al. [31] in connection with the study on the shape of the displacement spectrum. It was shown that the basic features of the displacement spectrum at long periods depend on the shape of the displacement pulse rather than on its derivatives, particularly the acceleration trace.

As such, the use of idealized simple pulses (Fig. 8) offers an advantage in modeling near-fault ground motion for design purposes (Sasani and Bertero [64]; Alavi and Krawinkler [4]; Kalkan and Kunnath [44]; Bhagat et al. [10]). The normalized acceleration, velocity, and displacement of the idealized simple pulse shape and the associated 5 and 30% damped response spectra are provided, respectively, in Figs. 8 and 9.

As it can be assessed, the key parameters involved in the definition of the pulse shapes shown in Fig. 8 are the amplitudes (PGA (A1), PGV, and PGD, which are all related) and the pulse period (Tp). Several researchers (e.g., Alavi and Krawinkler [3]; Mavroeidis
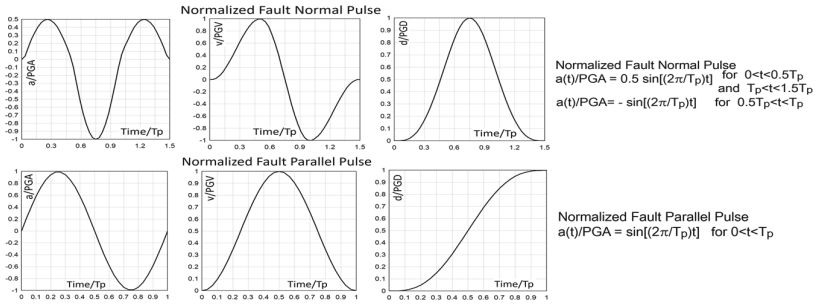
**Fig. 8.** Idealized sinusoidal fault normal (forward-directivity) and fault parallel (fling-step) pulses, normalized by maximum acceleration, velocity, and displacement.
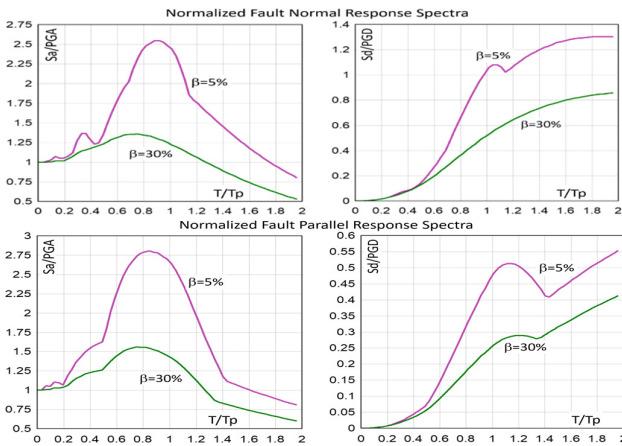


**Fig. 9.** The normalized 5 and 30% damped acceleration and displacement spectra are associated with the fault normal and fault parallel pulse shapes in Fig. 8.

and Papageorgiou [48]; Bray and Rodriguez-Marek [15]; Somerville [70]; Tang and Zhang [81]; Chen et al. [24]) have studied the relationship between pulse periods and magnitudes, and proposed some empirical models, which are plotted in Fig. 10. It can be assessed that in general, for all site conditions the pulse period has a range between 2 and 5 s for Mw between 7.0 and 7.5, where, the variation of Tp between site conditions is only about 20%. This Tp range almost totally covers the isolated period of vibration range for isolated structures.

Bray and Rodrigues-Marek [15] have thoroughly evaluated the variation of PGV with the earthquake magnitude and site conditions and have shown that the PGV in the near-fault region varies significantly with magnitude and distance, and additionally, the PGV for soil sites is systematically larger than those at rocks sites.

Bray and Rodrigues-Marek [15] compared the proposed relationship for PGV with those developed by Somerville [71] and Alavi and Krawinkler [3]. They have indicated that Somerville [71] and Alavi and Krawinkler [3] propose a much stronger variation of PGV with magnitude compared to Bray and Rodrigues-Marek [15]. This difference
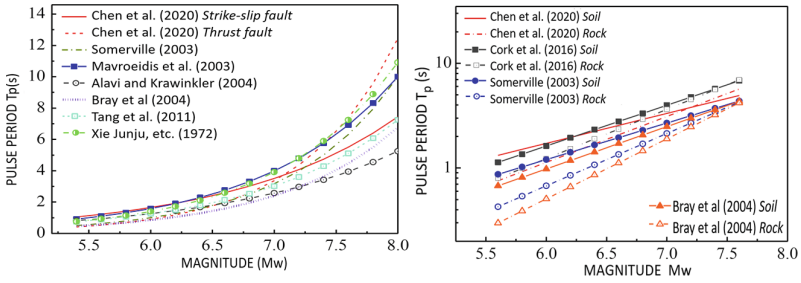
**Fig. 10.** Relationships between the pulse period (Tp) and the moment magnitude (Mw) (Chen et al. [24]).

essentially stems from the method of magnitude scaling and the amount of data included in the analysis. Chen and Wang [22] have shown that the peak pulse velocity (PGV) is only slightly related to the type of faulting and magnitude, as shown in the left pane of Fig. 11. In the right pane of Fig. 11, the variation of PGV with fault distance for and earthquake with magnitude Mw6 is indicated on the basis of regressions from different authors. It can be seen that Chen and Wang's [22] study yields the lowest values of PGV.
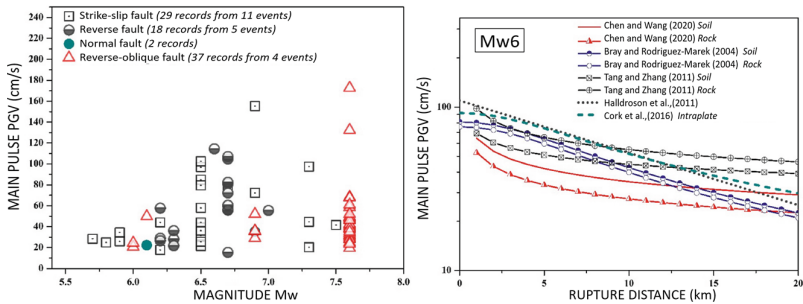


**Fig. 11.** Variation of PGV with the style of faulting, magnitude, and fault distance.

### 2.3.3 Ground-Motion Directivity Modelling for Seismic Hazard Applications

Probabilistic (hazard integral and Monte Carlo based) and deterministic procedures can be used for the hazard assessment (Donahue et al. [26]; Gentile and Galasso [34]). Donahue et al. [26], group these procedures under the main titles of A-Posteriori Modification and Incorporation of Directivity into Hazard Integral.

In the A-Posteriori Modification procedure, the results of the classical (directivity-neutral) PSHA are modified to approximately account for the directivity effects. A drawback of this procedure is that the resulting spectrum may not maintain the intrinsic probability level running PSHA with directivity-neutral GMMs and then modify the results in order to approximately account for directivity effects. For this modification, the following alternatives can be considered: (1) Composite Distribution Approach: which involves the deterministic changes in the mean and standard deviation after the hazard

deaggragation and the computation of the directivity modified spectral levels associated with each fault; (2) Scenario Event Incorporating Directivity Approach: applies to the conditional mean spectrum (CMS), which is computed for a scenario event identified through disaggregation of the hazard at a specific period, and its modification for the directivity effects. A-Posteriori Modification is adapted directly to UHS, where a single fault dominates the hazard for long periods if the hypocenter is assumed in a conservative manner (Donahue et al. [26]).

In the Incorporation of Directivity into Hazard Integral procedure, the classical hazard integral is extended to incorporate the directivity effects by considering the variability of the location of the hypocenter. This variation is achieved through Modified Moments from Randomized Hypocenter, which modifies the mean and standard deviation of ground motion to approximately account for the effect of variable hypocenter location; Directivity Parameter Randomization, which provides integration over a location-specific distribution of the directivity parameter, indirectly accounting for the variable hypocenter location and; Hypocenter Randomization, which results in integrating directly over alternate hypocenter locations (Donahue et al. [26]).

In addition to several hazard assessment software, the OpenQuake-engine (an open software for seismic hazard and risk assessment) is extended the ordinary hazard integral by adding two additional aleatory variables, hypocenter location and slip angle, to support the near-fault directivity effect (Chen et al. [23]).

## 3  Performance of Seismically Isolated Buildings Exposed to Near Fault Ground Motion

Extensive studies are conducted for the investigation of the response of conventional (non-isolated) buildings under exposure to near-fault ground motion. As expected, these studies have generally shown that the structural response is maximized in the fundamental period the structure is near the FD pulse period. The ground motions with FD pulses generate high demands that necessitate the dissipation of this input energy with few large displacement excursions, which increases the risk of brittle failure for poorly designed systems.

The presence of FD velocity pulses in the ground motions has been known to impose larger demands on structures than ground motions without velocity pulses (e.g. Almufti et al. [5]; Kitayama and Constantinou [46]; Sasani and Bertero [64]). Using displacement response spectra of idealized and recorded pulse-type ground motions, Sasani and Bertero [64] have shown the efficiency of added damping in controlling the response of multi-degrees of freedom systems acted upon by near-fault ground motion.

The study of Kalkan and Kunnath [45] on the response of steel moment frames under near-fault ground motion excitation demonstrated that the severity of the demands is controlled by the ratio of the pulse to system period and the ground motion records with forward directivity resulted in more instances of higher-mode demand while records with fling-step displacement almost always caused the systems to respond primarily in the fundamental mode. Essentially all of these findings necessitate an explicit consideration of pulse-type ground motions in the design of structures for near-fault conditions. Hall and Ryan [39] investigated the seismic performance of seismically isolated buildings

designed per the 1997 Uniform Building Code (UBC). The study indicated that seismically isolated moment-resisting frame buildings under exposure to near-fault ground motions could experience large inter-story drifts that can be controlled with supplemental dampers in the isolation system. Vassiliou et al. [76] and Bao et al. [9] studied the response of isolated structures under pulse-like ground motions and reported the dependence of the structural response on the pulse period. The behavior of base-isolated buildings under near-fault ground motions with fling-step and forward-directivity characteristics is investigated by Bhagat et al. [10] using a 10-story base-isolated building with and without shear walls. Their results indicate lower values of peak inter-story drift ratio for the buildings with shear walls compared to those with moment-resisting frames. The displacement demand at the isolation interface is maximum when the fundamental period of vibration of the building is equal to the pulse period.

Pant and Wijeyewickrema [55] studied the seismic pounding performance of typical four-story base-isolated RC buildings to near-fault ground motions with pulse-like nature. It is found that the peak base displacements under near-fault ground motions are 1.5–1.6 times larger than those under far-fault ground motions., where both ground motion sets are scaled to the same ASCE 7-10 MCER spectrum.

Kitayama and Constantinou [46] have investigated the collapse risk of seismically isolated buildings designed by the procedures of the ASCE/SEI 7-16 standard. The buildings are six-story perimeter frame buildings with special concentrically braced frames located at sites within 5 km of an active fault. The seismic isolation systems are comprised of: (i) triple friction pendulum bearings with high friction coefficients, (ii) triple friction pendulum bearings with the low friction coefficient and viscous dampers, and (iii) triple friction pendulum bearings with low friction coefficients. The paper demonstrated that seismically isolated buildings with either increased isolator displacement capacity or increased superstructure strength compared to the code-based minima could achieve an acceptable collapse risk. Furthermore, the seismic isolation systems that have the best collapse performance for far-field motions are not necessarily the best for near-fault ground motions. The results of Kitayama and Constantinou's [46] study also show that the probabilities of collapse have small differences for the three isolated buildings under exposure to near-field ground motions, while building with the high friction isolation system have the least collapse risk. The behavior of high-damping rubber bearings for base-isolated buildings under earthquake records, under exposure to horizontal impulsive ground motion together with either a pulse-like or a non-pulse-like vertical shaking, were studied by Quaranta et al. [60]. Results show that the maximum displacement of elastomeric bearings is moderately amplified and that significant negative effects on axial capacity, shear strain, and overall stability of elastomeric bearings can occur when the pulse-like vertical excitation is considered in the analysis.

## 4 Consideration of Near-Fault Ground Motion in Codes

Design codes and their reference standards describe how to design and detail structures in a prescriptive way. Code provisions have historically been developed based on recorded ground motions not sufficiently close to the causative fault. Thus, in general, the current seismic design codes do not explicitly provide an adequate representation of near-fault

ground motions. The codes and the earthquake-resistant design practice rely on response spectrum concepts where near-fault characteristics of ground motions are not provided sufficiently (Sommerville [17]; Shahi and Baker [66]; Akkar et al. [82]).

Distinguishing characteristics of near-fault ground motions were not implemented to design codes until the establishment of the 1990 SEAOC Blue Book. Base isolation Subcommittee of the Northern Section of SEAOC has developed N factors, and later, these proposed factors were adopted for the 1997 UBC.

In UBC 1997, the site-source and distance-dependent near-source factors (NA and NV) are introduced on the basis of fault types and fault distances to amplify the elastic design spectrum (i.e., the design base shear). The Na and Nv factors are applied uniformly over respective acceleration and velocity domains. For fault (A-Type) distances less than 2 km, this amplification varies between 50 and 100%. Needless to say, the rationality of constant amplification factors in providing reliable performance levels to near-fault structures are questionable.

For the incorporation of near-fault effects, approaches similar to UBC 1997 are also employed in the Chinese (Chai et al. [21]) and Taiwanese (Li et al. [47]) seismic design codes. The EN Eurocode 8 EN, Part 1 general provisions for near-source effects, does not exist. Part 2 of EC8 ("Bridges") requires, though, the use of site-specific spectra, taking into account near-source effects for bridges located within 10 km of a fault that can produce an earthquake with magnitude => Mw6.5.

New Zealand Standard NZS 1170.5 (2004) uses a near-fault factor (N (T, D)) in the definition of the elastic response spectra to account for near-source effects on the strong motion during the activation of a strike-slip fault: a) forward directivity, resulting in high peak velocities and displacements, and b) polarization of the long-period motions in the near-source region. The near-fault factor must be for sites located within a distance (D) less than 20 km from the major strike-slip faults, for return periods greater than 250 years using the following equations and Table 2 for the maximum values of near-fault factor, Nmax(T).

$$N(T, D) = Nmax(T) \text{ for } D \leq 2km \tag{9}$$

$$N(T, D) = 1 + (Nmax(T) - 1) \cdot (20 - D)/18 \text{ for } 2\,km < D \leq 20\,km \tag{10}$$

$$N(T, D) = 1.0 \text{ for } D > 20\,km \tag{11}$$

**Table 2.** Maximum values of near-fault factor, Nmax(T)

| Spectral period, T(s) | Nmax(T) |
| --- | --- |
| < 1.5 | 1.0 |
| 1.5 < T < 4 | 0.24T+0.64 |
| 4 < T < 5 | 0.12T+1.12 |
| > 5 | 1.72 |

Provisions in ASCE 7-22 [2021] provide guidance on ground-motion selection in consideration of pulse-like ground motions and orientation of the maximum component of ground motion in the FN direction. However, no specific guidance was provided regarding accounting for directivityeffects on intensity measures. In Caltrans (2019), the design spectra for California Bridges are modified for directivity effects by increasing the spectral ordinated at periods larger than 1 s by a factor of 20%. This adjustment factor is applied at locations with a site to rupture plane distance (RRUP) of 15 km or less and linearly tapered to no adjustment at 25 km. The adjustment consists of a 20% increase in spectral values with a corresponding period longer than one second. This increase is linearly tapered to zero at a period of 0.5 s. Since the design spectrum is probabilistically based and includes the influence of multiple faults, the site to rupture plane distance is based on the de-aggregated mean distance for spectral acceleration at a period of 1.0 s.

## 4.1 ASCE/SEI 7-22 (Near-Fault Ground Motion and Seismic Isolation Design)

In the current ASCE/SEI 7-22 (and also in ASCE/SEI 7-16) standard, the seismic design of seismically isolated structures (Chapter 17) is based on the MCER event only. The response reduction factor can have a maximum value of 2, thereby ensuring that the structure does remain essentially elastic at the MCER level. These standards stipulate that seismically isolated buildings located at near-fault sites should be designed by considering greater seismic demands (than the demand on structures at far-field sites) by using a larger spectral acceleration. For design under near-fault conditions, each pair of horizontal near-fault ground motion components shall be rotated to the fault-normal (FN) and fault-parallel directions (FP) of the causative fault and applied to the building in such orientation.

The Risk-Targeted Maximum Considered Earthquake (MCER) Ground Motion, prepared by the USGS (https://asce7hazardtool.online/; https://doi.org/10.5066/F7N K3C76), incorporates: (1) A target risk of structural collapse equal to 1% in 50 years based upon a generic structural fragility, (2) Factors to adjust from a geometric mean to the maximum response regardless of direction and (2) deterministic upper limits imposed near large, active faults, which are taken as 1.8 times the estimated median response to the characteristic earthquake for the governing fault (1.8 is used to represent the 84th percentile response). A USGS web tool (https://doi.org/10.5066/F7NK3C76) can also be used to determine the MCER (mapped value earthquake hazard) for a specified location.

It should be noted that two metrics are used to characterize ground motion directionality: The RotD50 (essentially equal to the Geometric Mean-GeoMean of the two orthogonal horizontal ground motion components) and the maximum direction RotD100 (MaxDir, orientation independent) values for all orientations (Shahi and Baker [66]). RotD50 is the median value of response spectra of the two horizontal components projected onto all non-redundant azimuths. RotD100 (or maximum direction) is the 100th percentile (the largest possible) value of response spectra of the two horizontal components projected onto all non-redundant azimuths. ASCE-7 defines the design basis of ground motion (MCER) on the basis of the RotD100, which is computed from conversion factors applied to the RotD50-based earthquake hazard maps.

In ASCE/SEI 7-22 provisions, the stipulations and comments regarding the near-fault ground motion, as well as those related to response history analysis, are as follows:

*CHAPTER 11 SEISMIC DESIGN CRITERIA*
*11.4.1 Near-Fault Sites satisfying either of the following conditions shall be classified as a near fault:*
*• 15 km or less from the surface projection of a known active fault capable of producing Mw7 or larger events, or*
*• 10 km or less from the surface projection of a known active fault capable of producing Mw6 or larger events.*
*EXCEPTIONS: 1. Faults with an estimated slip rate less than 1 per year shall not be used to determine whether a site is a near-fault site. 2. The surface projection used in the determination of near-fault site classification shall not include portions of the fault at depths of 10 km or greater.*
*CHAPTER 16 NONLINEAR RESPONSE HISTORY ANALYSIS*
*16.2.2 Ground Motion Selection*
*A suite of not less than 11 ground motions shall be selected for each target spectrum. Ground motions shall consist of pairs of orthogonal horizontal ground motion components and, where vertical earthquake effects are considered, a single vertical ground motion component. For near-fault sites, as defined in Section 11.4.1, and other sites where MCER shaking can exhibit directionality and impulsive characteristics, the proportion of ground motions with near-fault and rupture directivity effects shall represent the probability that MCER shaking will exhibit these effects.*
*16.2.3 Ground Motion Modification*
*Spectral matching shall not be used for near-fault sites unless the pulse characteristics of the ground motions are retained after the matching process has been completed.*
*16.2.3.2 Amplitude Scaling*
*For each horizontal ground motion pair, a maximum-direction spectrum shall be constructed from the two horizontal ground motion components.*
*16.2.4 Application of Ground Motions to the Structural Model*
*For near-fault sites, as defined in Section 11.4.1, each pair of horizontal ground motion components representative of a nearby fault source shall be rotated to the fault-normal and fault-parallel directions of the causative fault and applied to the building in such orientation.*

The modification of the MCER ground motion obtained from the code-associated seismic hazard map for the near-fault is not explicitly addressed in the ASCE/SEI 7 standards. In ASCE 7-22 [7], Chapter 21 (Site-Specific Ground Motion Procedures for Seismic Design) require that "*21.2.3 Site-Specific MCER Response Spectrum: The site-specific MCER spectral response acceleration at any period, SaM, shall be taken as the lesser of the spectral response accelerations from the probabilistic ground motions of Section 21.2.1 and the deterministic ground motions of Section 21.2.2*". Furthermore, C16.2.2 of ASCE 7-22 [7] (Ground Motion Selection) state that "the maximum direction of response tends to be in the direction normal to the fault strike."

In practical design applications following the ASCE 7-22 [7] Code, the following two methodologies are generally considered.

Methodology 1

(1a) PSHA-based MCER is calculated as per Chapter 21 through PSHA that incorporates directivity effects, summarized in Section 3.2.3 (RotD50) and then converted to (RotD100).

(1b) Develop probabilistic (2%/50) site-specific Fault Normal (FN) spectra through PSHA that incorporate directivity effects, summarized in Section 3.2.3.

(1c) For the probabilistic MCER, use the envelope of (1a) and (1b).

(1d) Compute the 84-percentile deterministic MCER: (RotD50), convert to (RotD100), and apply FN directivity modification.

(1e) Use the lesser of (1c) and (1d) (ASCE 7-22 [7] Ch. 21.2.3) to obtain the design basis MCER.

(1f) The Fault Parallel (FP) ground motion component represents the orthogonal component of horizontal ground motion required to achieve the Average Horizontal ground motion (RotD50 in 1a) when combined with the Fault Normal (FN) spectral ordinates. Noting that the geometric mean combination of the two orthogonal ground motion spectral amplitude components is used to obtain the Average Horizontal ground motion (RotD50), the Fault Parallel (FP) spectral components at each period (T) can be obtained by the FP(T) = [Average Horizontal(T)]2/[FN(T)] relationship.

Methodology 2

(2a) As an alternative to (1a), the ASCE 7-22 [7] code associated MCER (USGS supplied spectra) can be taken equal to the Fault-Normal (FN) ground motion component. The Fault-Normal (FN) ground motion is assumed to be equivalent to the maximum rotated component of ground motion (C16.2.2 of ASCE 7-22 [7]) and, therefore, represents the code definition of site-specific spectra (MCER),

(2b) The Average Horizontal ground motion represents the RotD50 ground motion,

(2c) The Fault Parallel (FP) ground motion component represents the orthogonal component of horizontal ground motion required to achieve the Average Horizontal ground motion when combined with the Fault Normal (FN) spectral ordinates. Noting that the geometric mean combination of the two orthogonal ground motion spectral amplitude components is used to obtain the Average Horizontal ground motion (RotD50), the Fault Parallel (FP) spectral components at each period (T) can be obtained by the

$$FP(T) = \big[\text{Average Horizontal(T)}\big]2/[\text{FN(T)}] \text{relationship.} \qquad (12)$$

The vertical ground motion spectrum will be based on the application of the vertical/horizontal (V/H) spectral amplitude ratios on the lesser of the PSHA and DSHA-based horizontal spectral response as per ASCE 7-22 [7] Section 21.2.3. For the application of V/H ratios, the RotD100 spectral metric needs to be converted to the RotD50 spectral metric through the use of conversion factors. The earthquake-resistant design of the Loma Linda Hospital (California) can be provided as a seismic isolation design example based on the 2nd Methodology. The Loma Linda University Medical Center (LLUMC) Replacement Hospital (Fig. 12) is a 17-story high steel frame 3-D seismically

isolated 100,000 square meters acute care hospital located 1 km from the M7.9 capable
San Jacinto Fault (Nielsen et al. [52]; Nielsen et al. [53]; Nielsen et al. [51]).
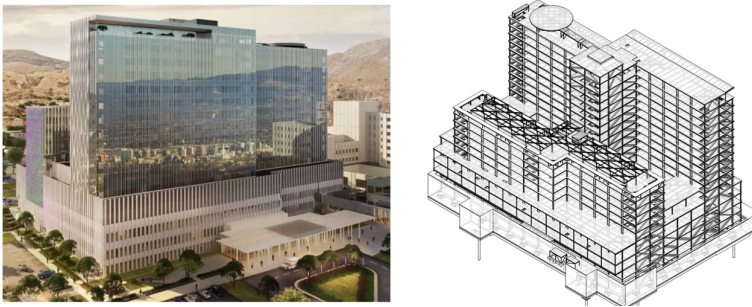


**Fig. 12.** Picture and an isometric view of the structure LLUMC hospital building.

The design basis response spectra prepared following ASCE 7-16 [6] site-specific
MCER specifications are provided in Fig. 13 (Courtesy of A. Dinsick, GeoPentech Inc.).
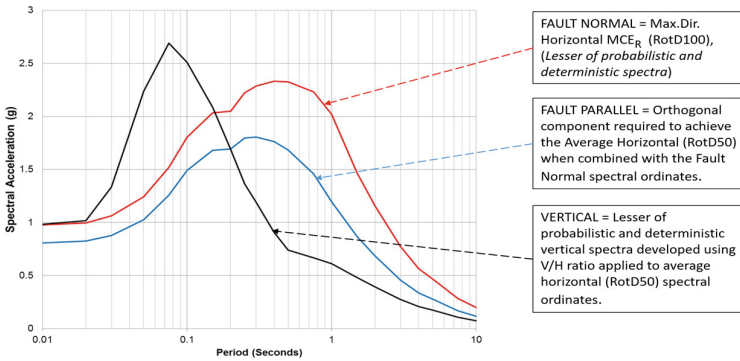


**Fig. 13.** LLUMC design basis response spectra prepared following ASCE 7-16 [6] site-specific
MCER specifications.

The following observations are in order:

- The response spectrum at Maximum Considered Earthquake (MCER) is given
  for horizontal fault-parallel, horizontal fault-normal, and vertical ground motion
  directions.
- For use in nonlinear response history analysis and 11 sets of three-dimensional
  spectrally matched MCER ground motion time histories were generated.
- The ground motions selected included a high proportion of near-fault pulse-like
  features.
- The fault-normal MCE spectrum is above 1.0 g lateral spectral acceleration at the 2 s
  period, corresponding to a high spectral displacement demand for a tall building.

- This is exacerbated by the pulse-like nonstationary characteristics of the Project specific ground motions, which act to further increase the displacement demand when applied in the time domain to a nonlinear response history analysis of a yielding lateral system.
- The severe vertical ground motion remains above 1.0 g until approximately 2 Hz, where the vertical frequencies of the floor system and columns are between 4 and 10 Hz.

The lateral base isolation system is comprised of 126 triple friction pendulum bearings (Earthquake Protection Systems) and 104 fluid viscous dampers with 3.6 MN capacity (Taylor Devices). The friction pendulum bearings have a Lateral Displacement Capacity of 1082 mm, Elastic Vertical Load Capacity of 36 MN, and provide an effective period of 4.5 s (Fig. 14). The total equivalent system damping coefficient is 50% of critical damping. The supplemental damping reduced the isolator displacement from 2137 to 1067 mm and greatly reduced the floor accelerations. To reduce the vertical ground motion being transmitted into the building, the vertical isolation system considered comprises an assembly of helical coil springs, fluid viscous dampers, and low-friction sliding shear pins mounted to a suspended concrete-filled steel pedestal.
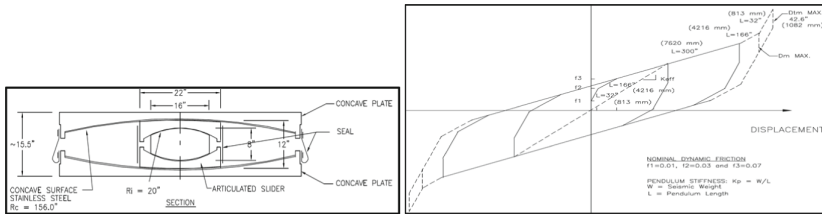


**Fig. 14.** Triple friction pendulum bearings (Earthquake Protection Systems) used in the isolation system (Courtesy of Dr. A. Mokha)

## 5 Parametric Study on Near-Fault Parametric Seismic Isolation Design (Earthquake Hazard)

### 5.1 Introduction

In this chapter, the response of the base-isolated buildings under near-fault (NF) ground motions with fling-step and forward-directivity characteristics are investigated with a rational assessment of design-basis near-fault ground motion, are investigated in a parametric format.

In this connection, we will consider a site with a site class qualified as "engineering bed-rock" with a Vs30 value of 760 m/s, located at a Joyner-Boore distance of Rjb = 2 km from the North Anatolian Fault as illustrated in Fig. 15. As it can be assessed the earthquake hazard at the site is totally controlled by the North Anatolian Fault.

## 5.2 Near-Fault Ground Motion Spectra

For the assessment of design basis near-fault ground motion spectra, we will consider a probabilistic approach and compute the UHS associated with the 2475-year average return period. The seismic source characterization is illustrated in Fig. 15. The 2475-year UHS for the site-class qualified as engineering bedrock (Vs30 = 760–800 m/s) is provided in Fig. 17 together with ESHM13 (Giardini et al. [35]; Giardini et al. [37]; Woessner et al. [78]) and ESHM2020 (Danciu et al. [25]) spectra for comparison purposes (Fig. 16).

For the incorporation of the near-fault effects on the 2475-year UHS, where a single fault dominates the hazard at long periods, the A-Posteriori Modification Method described in Chapter 2.4 (Donahue et al. [26]) will be considered. For this application, the 2475-year UHS is first subjected to a hazard deaggragation in the long period range, the controlling scenario earthquake is assessed, and the associated deterministic spectrum is developed to proxy the UHS.

The result of deaggragation analysis indicates an earthquake scenario defined by an Mw7.98 magnitude, Rjb = 2.5 km of rupture distance, and epsilon of $\varepsilon = 1.5$. The GMPEs considered in the first approach are also used in this approach to develop the %5 damped spectra. The Fault normal (FN), Fault Parallel (FP), and general direction ground motion spectra that reflect the directivity characteristic are computed using Bayles and Somerville's [56, 73] methodology. The acceleration spectra for FN, FP, and general direction (GeoMean) ground motion are provided in Fig. 18, associated with the scenario earthquake.
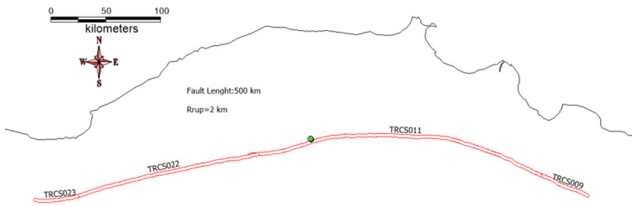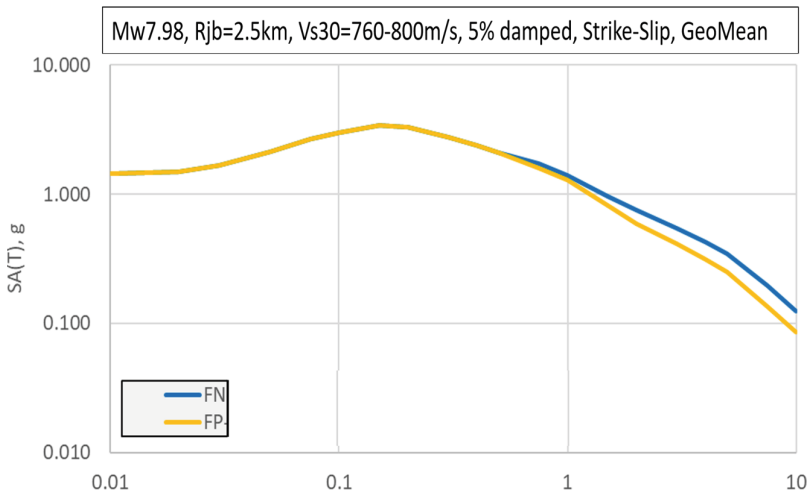


**Fig. 15.** Location of the site (green dot) at a distance of Rjb = 2 km from the North Anatolian fault.
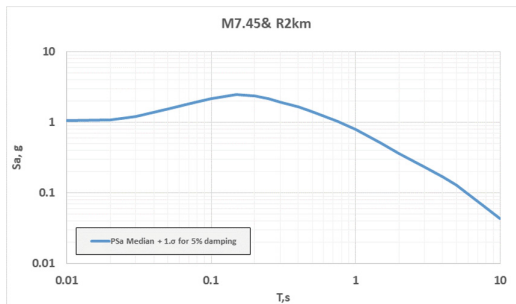


**Fig. 16.** Deterministic Median + 1 SD spectral acceleration.
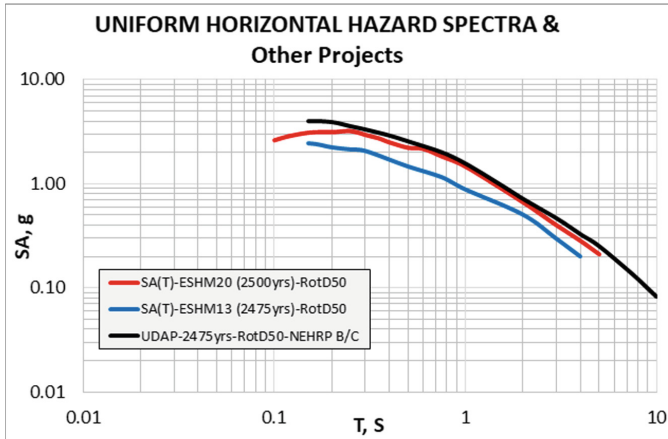
**Fig. 17.** The resulting 2475-year UHS for the site-class qualified as engineering bedrock together with ESHM13 (Giardini et al. [35]; Giardini et al. [37]; Woessner et al. [78]) and ESHM2020 (Danciu et al. [25]) spectra



**Fig. 18.** Acceleration spectra for FN, FP, and general direction (GeoMean) ground motion associated with the scenario earthquake and Median-1.5 SD.

## 5.3 Near-Fault Ground Motion in Time Domain (Pulse-Based)

As elaborated in Chapter 2.3.2, the NF ground motions with fling-step and forward-directivity characteristics can be identified from the velocity and displacement time histories. The forward directivity effect results in a large amplitude, long period two-sided pulse in the velocity time series of the FN component of the ground motion, whereas the fling step results in a one-sided velocity pulse and permanent displacement at the end of the ground motion record in the FP direction (along the fault plane, in the

direction of the slip). The pulse period and pulse amplitude are two major parameters of ground motion records having a velocity pulse. In this study, three pulse periods (Tp = 3, 4, and 5 s) obtained from the relevant references (Bray and Rodrigues-Marek [15]; Alavi and Krawinkler [3]; Sommerville [71]; Bray et al. [14]) are used. We believe that this pulse period range is valid for maximum magnitude in the range between Mw7.0 and Mw7.6.

The algorithm used in the pulse-based near field ground motion approach is shown in Fig. 19, and the acceleration, velocity, and displacement pulses for FN and FP corresponding to the three different pulse periods are presented in Fig. 20.
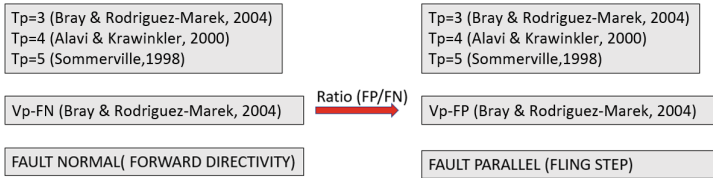


**Fig. 19.** The algorithm used in the pulse-based near field ground motion approach
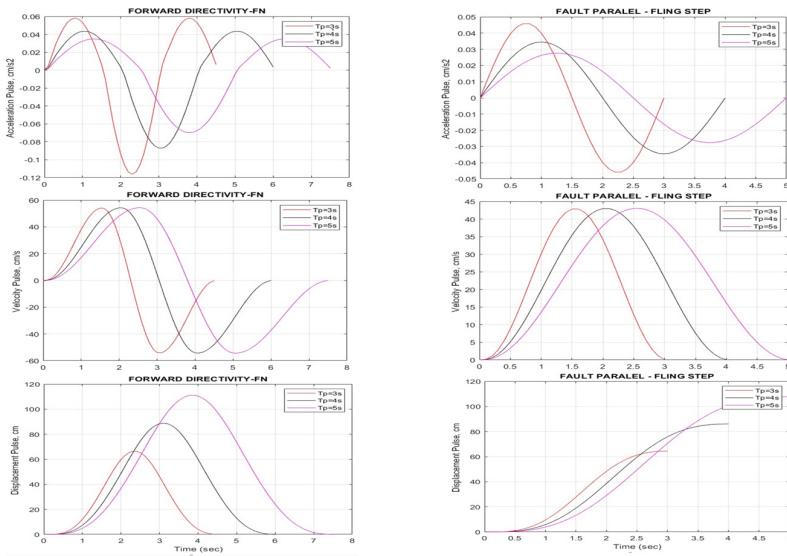


**Fig. 20.** The acceleration, velocity, and displacement pulses for FN and FP correspond to the three different pulse periods of 3, 4, and 5 s.
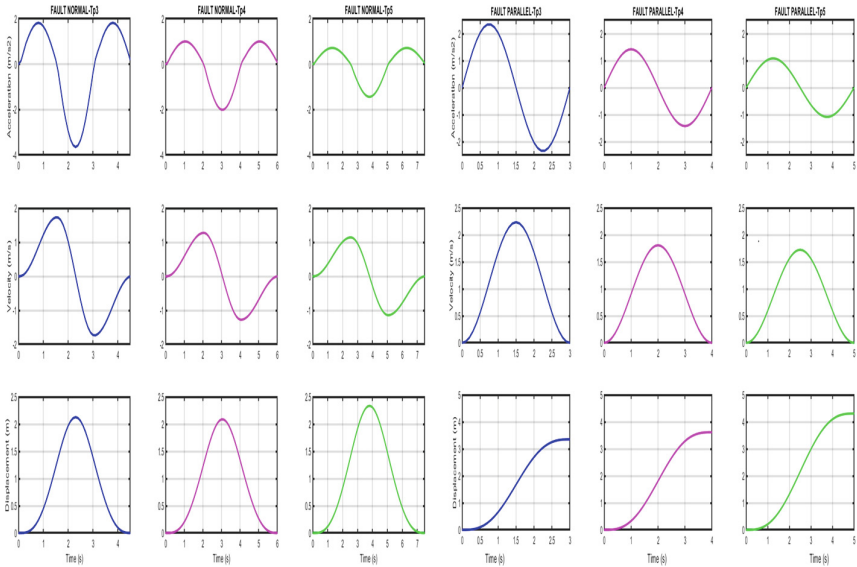
### 5.4 Spectrum Scaled Accelerometric Data

The set ground motions developed in Sect. 5.3 (Fig. 20) are used to develop the scaled accelerometric data compatible with the FN and FP spectra provided in Fig. 21. Figure 22

provides the comparison of the target and scaled ground motion spectra, and the acceleration, velocity and displacement spectra associated with the scaled accelerometric data provided in Fig. 23. As it can be assessed, the PGA and PGV amplitudes of these pulse-type ground motion respectively varies between 150 and 350 cm/s$^2$ and 110–160 cm/s for the pulse periods of $T_p = 3$, 4 and 5 s. PGA and PGV values in these ranges were observed in the following past strike-slip earthquakes (Mavroeidis and Papageorgiou [48]).

1971 Mw6.6 San Fernando (CA): PGA $= 400$ cm/s$^2$, PGV $= 130$ cm/s, $T_p = 2$ s.
1992 Mw6.6 Erzincan (Turkey): PGA $= 180$ cm/s$^2$, PGV $= 67$ cm/s, $T_p = 2$–3 s.
1999 Mw7.4 Kocaeli (Turkey): PGA $= 80$ cm/s$^2$, PGV $= 92$ cm/s, $T_p = 4$–5 s.
1979 Mw6.5 Imperial Valley (CA): PGA $= 160$ cm/s$^2$, PGV $= 96$ cm/s, $T_p = 3$–4 s.
1989 Mw6.9 Loma Prieta (CA): PGA $= 110$ cm/s$^2$, PGV $= 60$ cm/s, $T_p = 3$ s.
1992 Mw7.2 Landers (CA): PGA $= 100$ cm/s$^2$, PGV $= 61,000$ cm/s, $T_p = 4$ s.



Fig. 21. The FN and FP spectrum compatible scaled accelerometric data.

# 6 Parametric Study on Near-Fault Parametric Seismic Isolation Design (Structural Analysis)

## 6.1 Introduction

The near fault performance of seismically isolated buildings, subjected to the fault normal and fault parallel time histories developed in Chapter 5, were investigated through a parametric study.
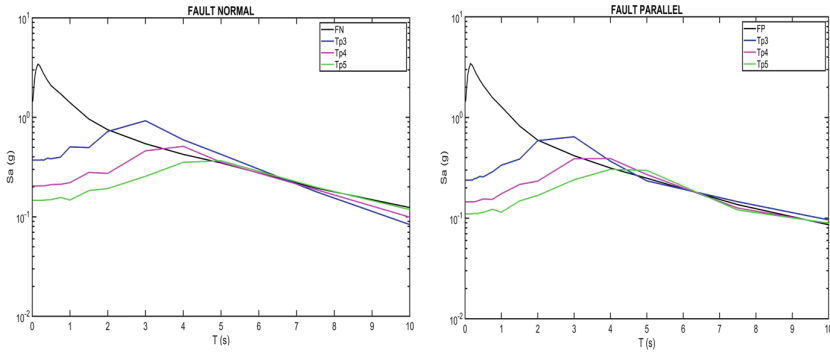
**Fig. 22.** Comparison of target and scaled-acceleration spectra for FN and FP ground motion.
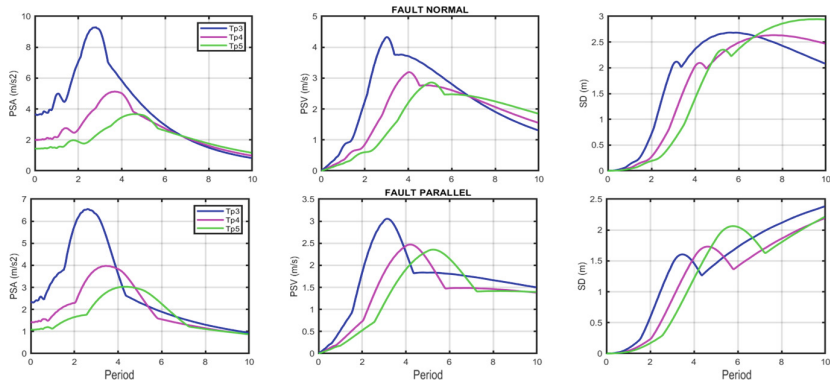


**Fig. 23.** The acceleration, velocity, and displacement spectra associated with the accelerometric data provided in Fig. 20.

The parametric study includes variables concerning the number of stories, structural system stiffness, and the isolation system characteristics (initial stiffness (K1), yield strength ($F_y$), and post-elastic stiffness (K2)). The nominal isolation period Ti is defined in terms of a rigid superstructure and the post-elastic stiffness, K2. The effect of supplemental damping in the isolation system by viscous dampers was also tested for some selected cases, and the performance of the structural system with and without the supplemental dampers was compared to demonstrate the need for additional damping systems.

## 6.2   Structural and Seismic Isolation Modelling

Lumped mass stick models were created in ETABS [https://www.csiamerica.com/products/etabs], representing the buildings with three, five, and eight stories (Fig. 24a). The seismic weight lumped at each story level and at the base is 5000 kN. The total seismic weight of an n-story building makes (n + 1) times 5000 kN (Table 3). The story heights were kept the same. Two different structural systems were considered, a frame system

representing a flexural structural system and a shear wall system representing a rigid structure.

**Table 3.** Structural model properties

| Number of stories | 3 | | 5 | | 8 | |
|---|---|---|---|---|---|---|
| Seismic weight of each story (kN) | 5000 | | 5000 | | 5000 | |
| Total seismic weight, W (kN) | 20,000 | | 30,000 | | 45,000 | |
| Structural system | Frame | Shear wall | Frame | Shear Wall | Frame | Shear wall |
| Fixed base period (s) | 0.5 | 0.3 | 0.75 | 0.45 | 1 | 0.6 |

A bilinear plastic link element (Fig. 24) is adopted to represent the seismic isolation system, with an initial elastic stiffness (K1), post elastic stiffness (K2), yield force (Fy), and a fixed yield displacement (Dy) of 0.015 m. Initial and post elastic stiffness are derived by the following Eqs. (13) and (14), where $T_i$ is the isolation period, and g is the acceleration of gravity. The yield strength ratio is varied between 4 and 10%, and the Ti is varied between 2.5 and 6 s. For the 3, 5, and 8-story buildings, fixed base first mode vibration periods of 0.5 s and 0.3 s; 0.75 s and 0.45 s; 1.0 s and 0.6 s are respectively considered. For each 3, 5, and 8-story building, the first period refers to a frame and the second period to a shear-wall type building.

$$K1 = \frac{F_y}{D_y} \tag{13}$$

$$K2 = \frac{4\pi^2 W}{gT_i^2} \tag{14}$$
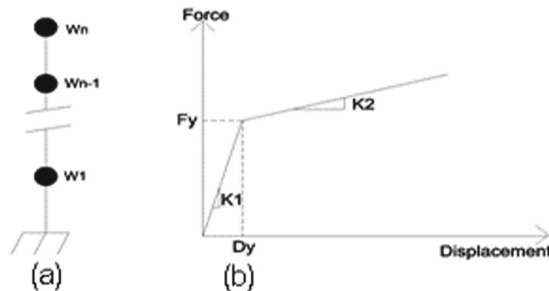


**Fig. 24.** Stick model representing the building structures (1) and bilinear force-displacement behavior of the seismic isolation system (2).

The models representing the building structure and the isolation system were excited with the three sets of accelerograms in fault normal and fault parallel directions associated

with three different pulse periods (Tp = 3, 4, and 5 s), as elaborated in Chapter 5. A direct integration method was employed. An intrinsic modal damping ratio of 2% is considered for the superstructure. A Multilinear plastic link element, following the hysteresis curve given in Fig. 24 (b), was considered to represent the isolation system. The isolation system displacement and base shear were obtained as the vectorial sum of the fault normal and fault parallel components. The mean (average) response associated with the three sets of accelerograms, in fault normal and fault parallel directions, is considered the demand.

## 6.3   Observation of the Parametric Response

### Effect of Superstructure Characteristics on the Seismic Isolation System Response

A parametric study was conducted to investigate the effect of the number of stories (3, 5, and 8) and the superstructure stiffness on the isolation system performance in terms of displacement, base shear, story drifts, and story accelerations while keeping the isolator properties constant ($F_y$ = 5% of W and $T_i$ = 4.0 s). The term "Shear Wall" is used to represent a stiff, while "Frame" is used to represent a flexible structural system. The mean responses were plotted in Fig. 25.
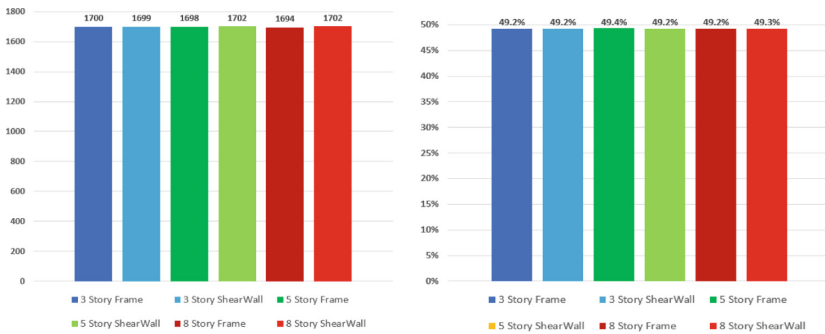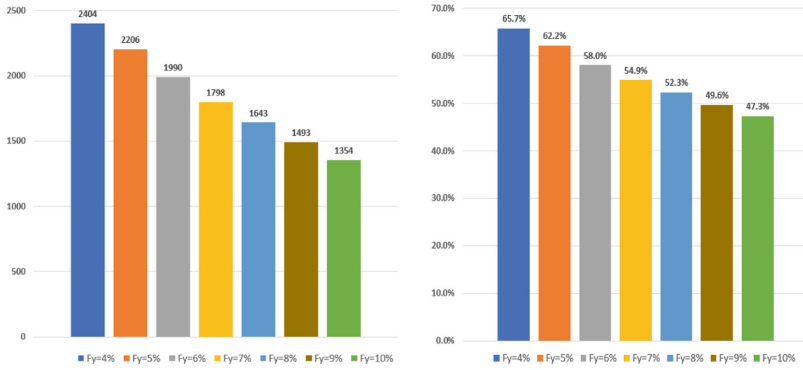


**Fig. 25.** Mean isolation system displacements and the base shear ratios.

### Effect of Seismic Isolation System Yield Force Ratio on Seismic Isolation System Response

A parametric study was conducted to investigate the effect of the seismic isolation system yield force (4, 5, 6, 7, 8, 9, and 10% of the total seismic weight) on the isolation system in terms of displacement, base shear, story drifts, and story accelerations for the five-story frame building. The post elastic stiffness of the seismic isolation system is kept constant, corresponding to an isolation period of $T_i$ = 4.0 s. The mean responses were plotted in Fig. 26.

### Effect of Seismic Isolation System Post-Elastic Stiffness on Seismic Isolation System Response

**Fig. 26.** Mean isolation system displacements and base shear ratios.

A parametric study was conducted to investigate the effect of the seismic isolation system post elastic stiffness (measured as Ti = 2.5, 3.0, 3.5, 4.0, 4.5, 5.0, 5.5, and 6.0 s) on the isolation system performance in terms of displacement, base shear, story drifts, and story accelerations for the five-story frame building. The yield force of the seismic isolation system is kept constant, corresponding to 5% of the total seismic weight. The mean responses were plotted in Fig. 27.
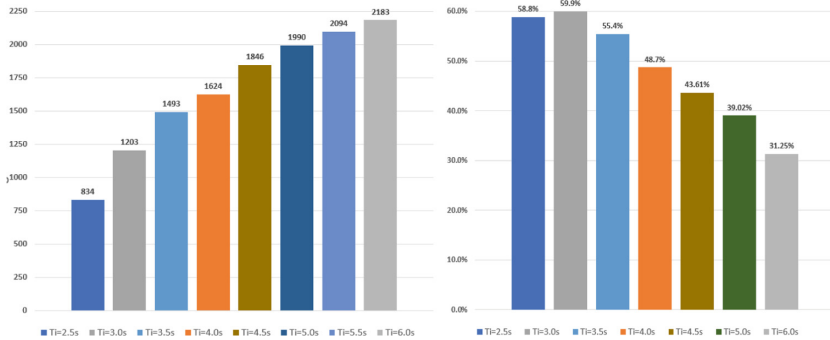


**Fig. 27.** Mean isolation system displacements and base shear ratios.

### Comparison of ELF Analysis and NLTHA Results

In Fig. 28, the ELF and NLTHA results were compared in terms of displacement and base shear for the five-story frame building with constant isolation system properties (Fy = 5% of W and Ti = 4.0 s).

ELF results vary according to the damping modification factors proposed in EC8 [20], TBDY [74], and ASCE 7/22 [7].

The damping modification factor proposed by Priestley et al. [58] for near-fault sites was also included in the comparison (Fig. 28).

### Effect of Supplemental Viscous Damping on Seismic Isolation System Response
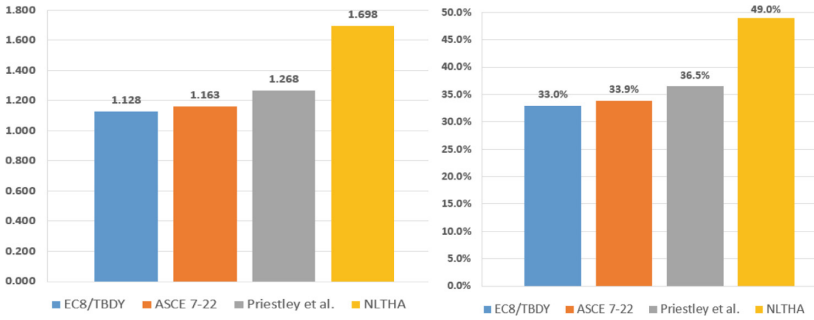
**Fig. 28.** Mean isolation system displacements and base shear ratios calculated by ELF method and NLTHA.

The seismic isolation system and seismically isolated building performance results in terms of isolation system displacement, base shear, story drifts, and top story acceleration were compared for the five-story flexible building structural system case with constant yield force and varying isolation period with and without supplemental viscous damping at isolation interface. The damping force (F) equation is given in Eq. (15), where V is the ground motion velocity, C is the damping constant taken as 600 kNs/m and α is the damping exponent considered 0.5.

$$F = CV^{\alpha} \tag{15}$$

The effect of supplemental viscous damping on the mean isolation system displacements and the base shear ratios are illustrated respectively in Figs. 29 and 30.
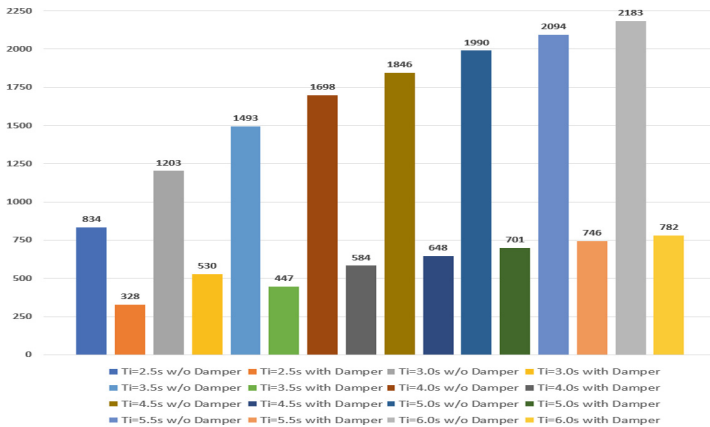


**Fig. 29.** Effect of supplemental viscous damping on mean isolation system displacements.
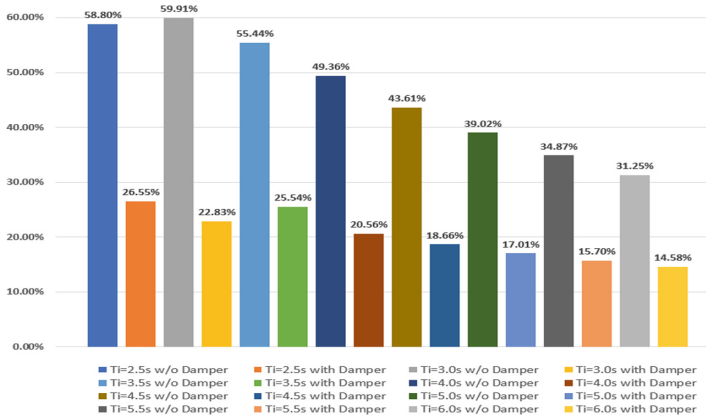
**Fig. 30.** Effect of supplemental viscous damping on mean base shear ratios.

## 7 Discussion and Conclusions

For base isolated structures the rational (i.e. state-of-the-art) determination of the long period region of the design basis ground motion is of particular importance due to associated structural safety and the isolation system cost implications. This importance becomes even more crucial for structures exposed to near-fault ground motion effects, since for Mw7-Mw7.5 earthquakes the dominant low frequency pulse period of the near-fault ground motion ($T_p = 3$–$5$ s) happens to coincide with the typical isolation period of vibration for almost all of the base isolated structures.

In only a few earthquake resistant design codes, the guidelines for the estimation of the near-field ground motion exist (some of which are now outdated) for the modification of the general horizontal direction (RotD50) conventional code-based design spectra. As far as known, the regulations regarding the design of the seismically isolated structures exist only in ASCE SEI 7 codes which stipulate the separate and direction associated application of fault-normal and fault-parallel components of the near-fault design basis ground motion.

This paper presents a review of the current methodologies for the assessment of the near-fault ground motion both in the frequency and time domains, as well as a critical summary of relevant design code regulations. A special study is conducted to find the effect of the near-fault ground motion on the response of a set of base isolated buildings with parameterized characteristics. As it can be observed from the normalized fault-normal (FN) and fault-parallel (FP) near-fault simple pulse-type ground motion spectra presented in Fig. 9, the amplification of the peak ground acceleration (PGA) and the peak ground displacement (PGD), within the normalized period range of $T_p = 0.8$–$1.2$, vary respectively between 2.2(FN)–2.6(FP) and 1.0(FP)–0.45(FP) for the damping ratio of $\beta = 0.05\%$. These amplifications drop down respectively to 1.2(FN)–1.4(FP) and 0.5(FP)–0.25(FP) for the damping ratio of $\beta = 0.05\%$ (a common value for seismic isolation systems). It should be noted PGA and PGV refer to the long period ($>= 3$ s) of the ground motion and that these amplification levels are applicable to the base of the

superstructure for base isolated structures with comparatively rigid superstructure with respect to the isolation system.

The special parametric study investigated the effects of superstructure characteristics, seismic isolation system yield force ratio, post-elastic stiffness and supplemental viscous damping on the seismic isolation system response. Furthermore, a comparison of ELF analysis and NLTHA results is conducted. The major finding of the special parametric study and conclusions drawn from this study are as follows.

- The main conclusion derived from the analysis of different superstructure and different isolation system properties, is that the maximum response is obtained from the fault-normal component of the ground motion.
- The number of stories and the type (frame of shear wall) of the superstructure does not significantly affect the isolation system displacement and the associated base shear ratio.
- As expected, increasing the yield level ratio (thereby increasing the equivalent damping ratio) of the isolation system, results in a reduction in isolation system displacement and the associated base shear ratio.
- As expected, the addition of viscous dampers substantially reduces the isolation system displacements and the associated base shear ratio, regardless of the number of stories and type of the superstructure and yield level ratio.
- The isolation system displacement and base shear ratio computed on the basis of the Effective Lateral Load (ELF) analysis indicate significant under estimation (in the order of 30%) compared to the Nonlinear Time History Analysis (NLTHA).
- Under near-fault conditions and soft soil sites the maximum vertical spectral amplitude can exceed even two times the corresponding general direction (RotD50) horizontal acceleration spectrum amplitude in short periods (0.05–0.1 s). As such, in near-fault conditions, both the isolation system elements and the superstructure are highly vulnerable and require careful consideration of the vertical ground motion excitation for safe design.
- Considering the results of basic design parameters such as isolation system displacement and base shear ratio, it can be deduced that, the design of the seismic isolation system under exposure to near-field ground motion requires the provision of supplemental damping to the system.
- The current seismic design codes do not explicitly provide an adequate representation of near-fault ground motions and only one (or few) of them provide limited guidelines for the design of base isolated structures in near fault conditions.
- In engineering practice, there is no generally accepted methodology for the design of the isolated structures exposed to near-field ground motion. We believe that the methodologies reviewed and developed in this paper will be useful for the design and/or the verification of design of base isolated structures in near fault conditions.

# References

1. Abrahamson, N.A., Silva, W.J., Kamai, R.: Summary of the ASK14 Ground-Motion Relation for active crustal regions. Earthq. Spectra (2014). https://doi.org/10.1193/070913EQS198M

2. Abrahamson, N.: Effects of rupture directivity on probabilistic seismic hazard analysis. In: 6th International Conference on Seismic Zonation, Earthquake Engineering Research Institute, CD-2000-01 (2000)
3. Alavi, B., Krawinkler, H.: Effects of near fault ground motions on frame structures. Report TR138, John A. Blume Earthquake Engineering Center. OCLC No. 48748468 (2001)
4. Alavi, B., Krawinkler, H.: Behaviour of moment resisting frame structures subjected to near-fault ground motions. Earthquake Eng. Struct. Dyn. **33**, 687–706 (2004)
5. Almufti, İ., Motamed, R., Grant, D.N., Willford M.: Incorporation of velocity pulses in design ground motions for response history analysis using a probabilistic framework. Earthquake Spectra (2015)
6. ASCE 7-16: Minimum Design Loads for Buildings and Other Structures. American Society of Civil Engineers, USA (2016)
7. ASCE/SEI 7-2022: Minimum Design Loads and Associated Criteria for Buildings and Other Structures. ASCE, NY (2022)
8. Baker, J.W.: Quantitative classification of near-fault ground motions using wavelet analysis. Bull. Seismol. Soc. Am. **97**, 1486–1501 (2007)
9. Bao, Y., Becker, T., Hamaguchi, H.: Failure of double friction pendulum bearings under pulse-type motions. Earthquake Eng. Struct. Dyn. **46**(5), 715–731 (2017)
10. Bhagat, S., Wijeyewickrema, A.C., Subedi, N.: Influence of near-fault ground motions with fling-step and forward-directivity characteristics on seismic response of base-isolated buildings. J. Earthquake Eng. **25**(3), 455–474 (2021). https://doi.org/10.1080/13632469.2018.152 0759
11. Bommer, J.J., Elnashai, A.S.: Displacement spectra for seismic design. J Earthquake Eng. **3**(1), 1–32 (1999)
12. Bozorgnia, Y., Campbell, K.W.: Ground motion model for the vertical-to-horizontal (V/H) ratios of PGA, PGV, and response spectra. Earthq. Spectra **32**(2), 951–978 (2016)
13. Bozorgnia, Y., et al.: NGA-West2 research project. Earthq. Spectra (2014). https://doi.org/10.1193/072113EQS209M
14. Bray, B., Rodriguez-Marek, A., Gillie, J.L.: Design ground motions near active faults. Bull. New Zealand Soc. Earthq. Eng. **42**(1) (2009)
15. Bray, J.D., Rodriguez-Marek, A.: Characterization of forward-directivity ground motions in the near-fault region. Soil Dyn. Earthq. Eng. **24**(11), 815–28 (2004). https://doi.org/10.1016/j.soildyn.2004.05.001
16. CALTRANS: CALTRANS SEISMIC DESIGN CRITERIA VERSION 2.0. State of California Department of Transportation (2019)
17. Campbell, K.W., Bozorgnia, Y.: NGA ground motion model for the geometric mean horizontal component of PGA, PGV, PGD and 5% damped linear-elastic response spectra for periods ranging from 0.01 and 10.0 s. Earthq. Spectra **24**, 139–171 (2008)
18. Campbell, K.W., Bozorgnia, Y.: NGA-West2 ground motion model for the average horizontal components of PGA, PGV, and 5% damped linear acceleration response spectra. Earthq. Spectra (2014). https://doi.org/10.1193/062913EQS175M
19. Cauzzi, C., Faccioli, E., Paolucci, R.: A reference model for prediction of long period response spectral ordinates—deliverable D2 (Task 1), Politecnico di Milano (2007)
20. CEN: Eurocode 8: design of structures for earthquake resistance. prEN 1998-1 (Draft No. 6), Comité Européen de Normalisation, Brussels, Belgium (2005)
21. Chai, J., Loh, C., Chen, C.: Consideration of the near-fault effect on seismic design code for sites near the Chelungpu fault. J. Chin. Inst. Eng. **23**(4), 447–454 (2000)
22. Chen, X., Wang, D.: Multi-pulse characteristics of near-fault ground motions. Soil Dyn. Earthq. Eng. **137**, 106275 (2020). https://doi.org/10.1016/j.soildyn.2020.106275(2020)

23. Chen, Y., Pagani, M., Weatherill, G., Cotton, F.: Exploring near-fault directivity effect in probabilistic seismic hazard assessment. In: 16th World Conference on Earthquake, 16WCEE 2017 Santiago Chile, January 9th to 13th 2017 Paper N° 2337 (2017)

24. Chen, Y., Xu, L., Wu, P.: Low-cut filter frequency quantification and its influence on 21 inelastic response spectrum. J. Earthq. Eng. 1–25 (2021). 22 https://doi.org/10.1080/13632469.2021.1927900

25. Danciu, L., Nandan, S., Reyes, C., Basili, R., Weatherill, G., Beauval, C., Rovida, A., Vilanova, S., Sesetyan, K., Bard, P-Y., Cotton, F., Wiemer, S., Giardini, D.: The 2020 update of the European Seismic Hazard Model: Model Overview. EFEHR Technical Report 001, v1.0.0. https://doi.org/10.12686/a15 (2021)

26. Donahue, J.L., Stewart, J.P., Gregor, N., Bozorgnia, Y.: Ground-motion directivity modeling for seismic hazard applications. Review panel: Jonathan D. Bray, Stephen A. Mahin, I. M. Idriss, Robert W. Graves and Tom Shantz. PEER_2019/03 Report (2019)

27. Yang, Y., Zhang, J.: Response spectrum-oriented pulse identification and magnitude scaling of forward directivity pulses in near-fault ground motions. Soil Dyn. Earthq. Eng. 31(1), 59–76 (2011). https://doi.org/10.1016/j.soildyn.2010.08.006

28. EC-8: Design provisions for earthquake resistance of structure. Eurocode-8, European Committee for Standardization (1998)

29. EC8: Design provisions for earthquake resistance of structures publication ENV-2003-2. Comite European de Normalizations, Brussels (2003)

30. Erdik, M., Sestyan, K., Demircioglu, M., Tuzun, C., Giardini, D., Gulen, L., Akkar, S., Zare, M.: Assessment of seismic hazard in the Middle East and Caucasus: EMME (Earthquake Model of Middle East) project. In: Proceedingd of 15th World Conference on Earthquake Engineering, Lisbon, Portugal (2012)

31. Faccioli, E., Paolucci, R., Rey, J.: Displacement spectra for long periods. Earthq. Spectra 20, 347–376 (2004)

32. Fu, Q., Menun, C.: Seismic-environment-based simulation of near-fault ground motions. In: Proceedings of the 13th World Conference on Earthquake Engineering, Vancouver, Canada, 1–6 August, p. 15 (2004)

33. Quaranta, G., Angelucci, G., Mollaioli, F.: Near-fault earthquakes with pulse-like horizontal and vertical seismic ground motion components: analysis and effects on elastomeric bearings. Soil Dyn. Earthq. (2022)

34. Gentile, R., Galasso, C.: Hysteretic energy-based state-dependent fragility for ground-motion sequences. Eng. Struct. Dyn. 50, 1187–1203 (2021)

35. Giardini, D., et al.: Seismic Hazard Harmonization in Europe (SHARE): Online Data Resource (2013). https://doi.org/10.12686/SED-00000001-SHARE

36. Giardini, D., Danciu, L., Erdik, M., Sesetyan, K., Demircioglu, M., Akkar, S., Gülen, L., Zare, M.: Seismic hazard map of the middle east (2016). 10.12686/a1

37. Giardini, D., Woessner, J., Danciu, L.: Mapping Europe's seismic hazard. EOS 95(29), 261–262 (2014)

38. Gülerce, Z., Kamai, R., Abrahamson, N.A., Silva, W.J.: Ground motion prediction equations for the vertical ground motion component based on the NGA-W2 database. Earthq. Spectra 33(2), 499–528 (2017)

39. Hall, J.F., Ryan, K.L.R.: Isolated buildings and the 1997 UBC near-source factors. Earthq. Spectra 16(2) (2000)

40. Hall, J.F., Heaton, T.H., Halling, M.W., Wald, D.J.: Near-source ground motion and its effects on flexible buildings. Earthq. Spectra 11(4), 569–605 (1995)

41. Heaton, T.H.: Evidence for and implications of self-healing pulses of slip in earthquake rupture. Phys. Earth Planer. lmeriors 64, 1–20 (1990)

42. Donahue, J.L., et al.: Ground-motion directivity modeling for seismic hazard applications. PEER Report 2019/03 (2019)

43. Hall, J.F., Ryan, K.L.: Isolated buildings and the 1997 UBC near-source factors. Earthq. Spectra 16(2). https://doi.org/10.1193/1.1586118
44. Kalkan, E., Kunnath, S.K.: Effects of fling step and forward directivity on seismic response of buildings. Earthq. Spectra **22**(2), 367–390 (2006)
45. Kalkan, E., Kunnath, S.K.: Effects of fling step and forward directivity on seismic response of buildings. Earthq. Spectra **22**(2), 367–390 (2006)
46. Kitayama, S., Constantinou, M.: Performance evaluation of seismically isolated buildings near active faults. Earthq. Eng. Struct. Dyn. **51**(5)
47. Li, X., Dou, H., Zhu, X.: Response of seismic design code for zones lack of near-fault strong earthquake records. ACTA Seismol. Sinica **20**(4), 447–453 (2007)
48. Mavroeidis, G.P., Papageorgiou, A.S.: A mathematical representation of near-fault ground motions. Bull. Seismol. Soc. Am. **93**, 1099–1131 (2003)
49. Mavroeidis, G.P., Dong, G., Papageorgiou, A.S.: Near-fault ground motions, and the response of elastic and inelastic single-degree-freedom (2004)
50. Vassiliou, M.F., Tsiavos, A., Stojadinović, B.: Dynamics of inelastic base-isolated structures subjected to analytical pulse ground motions. Earthq. Eng. Struct. Dyn. **2013**(42), 2043–2060 (2013)
51. Nielsen, G., Rees, S., Dong, B., Chok, K., Fatemi, E., Zekioglu, A.: Practical implementation of ASCE-41 and NLRHA procedures for the design of the LLUMC replacement hospital. In: 2017 SEAOC Convention Proceedings (2017)
52. Nielsen, G., Sarebanha, A., Biscombe, L., Shao, B., Rees, S.: Development and experimental validation of a 3-D seismic isolation system using Ls-Dyna. In: 17th World Conference on Earthquake Engineering, 17WCEE (2020)
53. Nielsen, G., Rees, S., Zekioglu, A., Sarebanha, A., Biscombe, L., Shao, B., Dong, B.: A 3-D seismic isolation system to protect the Loma Linda University Hospital from near-fault earthquakes. In: 17th World Conference on Earthquake Engineering, 17WCEE (2020)
54. NZS 1170.5 Supp 1:2004. Structural Design Actions Part 5: Earthquake Actions-New Zealand-Commentary. Standards New Zealand (2004)
55. Pant, D.R., Wijeyewickrema, A.C.: Influence of near-fault ground motions on the response of base-isolated reinforced concrete buildings considering seismic pounding. Adv. Struct. Eng. **16**(12), 1973–1988 (2013)
56. PEER 2013 Report: Paul Spudich; Jeffrey R. Bayless; Jack W. Baker; Brian S.J. Chiou; Badie Rowshandel; Shrey K. Shahi; Paul Somerville. Final Report of the NGA-West2 Directivity Working Group, PEER Report 2013-09 (2013)
57. Donahue, J.L., Stewart, J.P., Gregor, N., Bozorgnia, Y.: Ground-motion directivity modeling for seismic hazard applications. PEER Report 2019/03 (2019)
58. Priestley, M.N.: Myths and Fallacies in Earthquake Engineering, Revisited: The Ninth Mallet Milne Lecture, p. 119. IUSS Press, Pavia, Italy (2003)
59. Priestley, M.J.N.: Seismic behaviour of unreinforced masonry walls. Bull. New Zealand Natl. Soc. Earthq. Eng. **18**(2), 191–205 (1985)
60. Quaranta, G., Angelucci, G., Mollaioli, F.: Near-fault earthquakes with pulse-like horizontal and vertical seismic ground motion components: analysis and effects on elastomeric bearings. Soil Dyn. Earthq. Eng. **160** (2022)
61. Gentile, R., Galasso, C.: Accounting for directivity-induced pulse-like ground motions in building portfolio loss assessment. Bull. Earthq. Eng. **19**(15), 6303–6328 (2020). https://doi.org/10.1007/s10518-020-00950-9
62. Rodriguez-Marek, A., Bray, J.D.: Seismic site effects for near-fault forward directivity ground motions. J. Geotech. Geoenviron. Eng. ASCE **132**(12), 1611–1620 (2006)
63. Rowshandel, B.: Directivity correction for the Next Generation Attenuation (NGA) relations. Earthq. Spectra **26**(2), 525–559 (2010). https://doi.org/10.1193/1.3381043

64. Sasani, M., Bertero, V.V.: Importance of severe pulse-type ground motions in performance-based engineering: historical and critical review. In: Proceedings of 12th World Conference on Earthquake Engineering, Paper No. 1302 (2000)
65. Bhagat, S., Wijeyewickrema, A.C., Subedi, N.: Influence of near-fault ground motions with fling-step and forward-directivity characteristics on seismic response of base-isolated buildings. J. Earthq. Eng. **25**(13), 455–447 (2021)
66. Shahi, S., Baker, J.W.: An empirically calibrated framework for including the effects of near-fault directivity in probabilistic seismic hazard analysis. Bull. Seismol. Soc. Am. **101**(2), 742–755 (2011)
67. Michael, S.K., Constantinou, C.: Performance evaluation of seismically isolated buildings near active faults. Earthq. Eng. Struct. Dyn. **51**(5), 1017–1037 (2022)
68. Somerville, P., Graves, R.: Conditions that give rise to unusually large long period ground motions. In: The Structural Design of Tall Buildings, vol. 2(3), pp. 211–232 (1993)
69. Somerville, G.P.: Near Fault Directivity Pulse Model: Development and Application in Scenario and Probabilistic Maps of Pulse Parameters in the San Francisco Bay Area. URS Greiner Woodward Clyde (2004)
70. Somerville, P.G.: Magnitude scaling of the near fault rupture directivity pulse. Phys. Earth Planet. Inter. **137**, 201–212 (2003)
71. Somerville, P.G., Smith, N.F., Graves, R.W., Abrahamson, N.A.: Modification of empirical strong ground motion attenuation relations to include the amplitude and duration effects of rupture directivity. Seismol. Res. Lett. **68**(1), 199–222 (1997)
72. Somerville, P.G., Graves, R.W.: Conditions that gives rise to unusually large long period ground motions. In: The Structural Design of Tall a Buildings, vol. 2, pp. 211–232 (1993)
73. Spudich, P., Bayless, J., Baker, J., Chiou, B.S.J., Rowshandel, B., Shahi, S., Somerville, P.: Final Report of the NGA-West2 Directivity Working Group (2013)
74. TBDY-2018: Türkiye Bina Deprem Yönetmeliği. https://www.resmigazete.gov.tr/eskiler/2018/03/20180318M1.pdf (2018)
75. Tothong, P., Cornell, C.A., Baker, J.W.: Explicit directivity-pulse inclusion in probabilistic seismic hazard analysis. Earthq. Spectra **23**(4), 867–889 (2007)
76. Vassiliou, M.F., Tsiabos, A., Stojabinovic, B.: Dynamics of inelastic base-isolated structures subjected to analytical pulse ground motions. Earthq. Eng. Struct. Dyn. (2013)
77. Veletsos, A.S., Newmark, N.M.: Response spectra for single-degree-of-freedom elastic and inelastic systems. Report No. RTD-TDR-63-3096, Vol. III, Air Force Weapons Lab., Albuquerque, N. Mexico (1964)
78. Woessner, J., et al.: The 2013 European seismic hazard model: key components and results. Bull. Earthq. Eng. **13**(12), 3553–3596 (2015). https://doi.org/10.1007/s10518-015-9795-1
79. Xinle, L., Huijuan, D., Xi, Z.: Engineering characteristics of near fault vertical ground motion and their effect on the seismic response of bridges. Earthq. Eng. Eng. Vib. **6**(4), 345–350 (2007)
80. Bao, Y., Becker, T.C., Hamaguchi, H.: Failure of double friction pendulum bearings under pulse-type motions. Eng. Struct. Dyn. **46**, 715–732 (2017)
81. Tang, Y., Zhang, J.: Response spectrum-oriented pulse identification and magnitude scaling of forward directivity pulses in near-fault ground motions. Soil Dyn. Earthq. Eng. **31**, 59–76 (2011)
82. Akkar, S., Moghimi, S., Arıcı, Y.: A study on major seismological and fault-site parameters affecting near-fault directivity ground-motion demands for strike-slip faulting for their possible inclusion in seismic design codes. Soil Dyn. Earthq. Eng. **104**(2018), 88–105 (2018)